Fault-controlled dolomitization in the Montagna dei Fiori Anticline (Central Apennines, Italy): Record of a dominantly pre-orogenic fluid migration

Mahtab Mozafari[1], Rudy Swennen[2], Fabrizio Balsamo[1], Hamdy El Desouky[2,3], Fabrizio Storti[1] and Conxita Taberner[4]

1- NEXT - Natural and Experimental Tectonics Research Group - Department of Chemistry, Life Sciences and Environmental Sustainability, University of Parma, Italy.

2- Department of Earth and Environmental Sciences, KU Leuven, Belgium.

3- Geology Department, Faculty of Science, Menoufia University, Menoufia, Egypt

4- Shell Global Solutions International B.V., Amsterdam, The Netherlands

Correspondence: Mahtab Mozafari (mahtab_mozafari@yahoo.com) and Fabrizio Storti (Fabrizio.Storti@unipr.it)

Abstract

The Lower Jurassic platform and basinal deposits exposed in the Montagna dei Fiori Anticline (Central Apennines, Italy) are pervasively affected by dolomitization. Based on the integration of field work, petrography, and geochemistry, two fault-related dolomitization events were recognized and interpreted as having occurred before and during the Apenninic orogeny, respectively. Fluid inclusion analysis indicates moderate to elevated salinity values of 3.5 to 20.5 and 12.8 to 18.6 eq. wt. % NaCl, in the first and the second event, respectively. The estimated salinities, in combination with $\delta^{18}O$ values and $^{87}Sr/^{86}Sr$ ratios, suggest significant involvement of evaporitic fluids in both events, most likely derived from the underlying Upper Triassic Burano Formation. In addition, the $^{87}Sr/^{86}Sr$ ratios up to 0.70963 suggest the circulation of deep-sourced fluids that interacted with ~~siliciclastics~~ siliciclastic rocks and/or the crystalline basement during the dolomitization events. ~~The first dolomitization event which is also considered as the most pervasive one started prior to the significant burial conditions, as reflected in homogenization temperatures of their fluid inclusions being mostly below about 40-50°C.~~

Two major dolomite types (D1 and D2) were recognized as pertaining to ~~this~~ the first event, both postdated by high amplitude bed-parallel stylolites~~.~~, supporting~~This relationship supports~~ a syn-burial, pre layer-parallel shortening dolomitization~~, interpreted as controlled by the extensional fault pattern affecting the carbonate succession before its involvement in the~~

~~Apenninic thrust wedge~~. A possible geodynamic framework for this dolomitization event is Early to Late Jurassic rift-related extensional tectonism. The second dolomitization event (D3, D4 and D5) ~~initiated with a dolomite type (D3)~~is characterized by a ~~slight~~ temperature upturn ~~(up to 73°C), followed by a second type (D4) with markedly higher homogenization temperatures~~ (up to 105°C), and interpreted as associated with the inflow of hydrothermal fluids, possibly related to major changes in the permeability architecture of faults during early- to syn-thrusting and folding activity. ~~Eventually, D4 was overprinted by a late generation of dolomite veins (D5) interpreted as associated with late orogenic extensional faulting in the backlimb of the Montagna dei Fiori Anticline.~~ Based on the timing of deformation in the Montagna dei Fiori Anticline, ~~D3 to D5~~the second dolomitization event likely occurred in Late Miocene to Pliocene times. The findings regarding characteristics and timing of dolomitization here illustrates the long-term controlling role of the ~~eveporitic~~ evaporitic detachments in dolomitization process. ~~Our data~~This study shows that the Mg-rich fluids that were most likely derived from ~~these~~ evaporites may prime the tectonically involved successions for repeated dolomitization, and hence formation of potential reservoirs ~~in~~ during sequential tectonic modifications (extensional vs. compressional).

1 Introduction

Fault-controlled dolomitization has been the focus of attention in many studies during the last decades due to its influential role in modifying the petrophysical properties of rocks and, hence, anisotropy in fluid migration pathways, and, ultimately on reservoir quality (e.g. Purser et al., 1994; Montanez, 1994; Zempolich and Hardie, 1997; Vandeginste et al., 2005; Davies and Smith, 2006; Sharp et al. 2010). The mechanical and hydrological behaviour of fault zones are in turn influenced by fluid-rock interactions and diagenetic modifications (e.g. Gale et al., 2004; Laubach et al., 2010; Clemenzi et al., 2015; Ferraro et al., 2019). It follows that the mutual interplay between fault activity and ~~fluid-driven~~ rock-fluid interaction can trigger dolomitization of carbonates when exposing to Mg saturated or oversaturated fluids and, consequently, variations in physico-chemical properties of fluids through time and space.

~~-~~Leaking or sealing behaviours of fault zones during deformation are key controls for fault-related fluid circulation. A detailed understanding of such an interplay is thus necessary to improve our capability of making reliable predictions of fault-related dolomitization in carbonate reservoirs. Studying outcrop analogues provides fundamental support to meet this requirement

~~(e.g. Swennen et al., 2012; Dewit et al., 2014; Bistacchi et al., 2015).~~, and the opportunity to assess the spatial distribution of dolomitized zones, and individual diagenetic events, in 3D (e.g. Swennen et al., 2012; Dewit et al., 2014; Bistacchi et al., 2015).

The Lower Jurassic to Lower Cretaceous Umbria-Marche passive margin carbonate succession, in the Central Apennines (Italy), is intensely affected by localized dolomitization both in the onshore fold-and-thrust belt and in offshore foredeep and foreland areas (e.g. Murgia et al., 2004; Pierantoni et al., 2013). The dolomitized intervals which are the focus of this study are well-exposed in the core of the Montagna dei Fiori Anticline ~~(e.g. Ronchi et al., 2003)~~, where the dolomitized Lower Jurassic intervals (Calcare Massiccio, Bugarone and Corniola Formations) and their relationships with fault zones allow to study the mutual influence between deformation structures and dolomitized intervals (Fig. 1). These intervals, known as the Castel Manfrino Dolostones (Crescenti, 1969; Mattei, 1987; Koopman, 1983), have been previously studied by Ronchi et al. (2003) only at its reference section, exposed at the Castel Manfrino location (Fig. 1b), in the central sector of the Montagna dei Fiori Anticline (Fig. 2). A fault-controlled dolomitization model and the relative timing of dolomitization were proposed by ~~Ronchi (2003)~~the latter authors~~.~~ based on the homogenization temperatures obtained from microthermometry of the fluid inclusions, and their relation with the thermal history of the area studied. However, no clear relation between dolomitization and structural evolution of the Montagna dei Fiori Anticline on a local scale was provided to confidently link the occurrence of dolomitization to a particular tectonic event. Moreover, the nature and origin of the dolomitizing fluids were not well constrained. Recent re-evaluation of dolostone distribution in the Montagna dei Fiori Anticline (Storti et al., 2017a), showed that the dimension of the dolomitized geobodies (Fig. 2) is much more significant than what was previously mapped by Mattei (1987). Dolostones are distributed within fault damage zones and in the laterally adjacent carbonate rocks, and in intersection areas between fault sets, for a total area in map view of more than 1.5 km^2 (Storti et al., 2017a).

The structural pattern of the Montagna dei Fiori Anticline documents the overprinting of extensional and contractional deformation along major fault zones. ~~Although challenging, the~~The preserved structural framework in this anticline provides an opportunity to study the direct but complex regional tectonic controls on dolomitization in carbonate successions undergoing multiple deformation events, from rifting to folding and thrusting. This contribution integrates

~~field mapping,~~ new petrographic, geochemical, and microthermometric analyses, with structural studies (Storti et al., 2018) to characterize the temporal record of fault-controlled diagenetic phases and, more specifically, dolomitization in the carbonatic succession outcropping in the Montagna dei Fiori Anticline. ~~Therefore provides insights into the structural controls on regional fluid flow and their chemical evolution through time.~~ These findings might be of relevance for exploration and reservoir quality prediction in the region of ~~onshore and offshore~~ the Apennines and Southern Alps, both onshore and offshore. Moreover, this work provides additional evidence of the potential influence of fluids derived from evaporitic detachment levels in modifications of geochemical trends and petrophysical properties of the overlying carbonate rocks.

2 Geological setting

The Montagna dei Fiori Anticline is a NNW-SSE striking, thrust-related fold located at the mountain front of the Central Apennines (Fig. 1). The geodynamic evolution of the Apennines ~~is generally known~~has been proposed to be the result of the superposition of NE-SW compression (in present-day geographic coordinates), related to the convergence between Eurasia and Africa plates since the Late Cretaceous times (Elter et al., 1975; Dewey et al., 1989; Patacca et al., 1992), on a rifting-related tectono-sedimentary architecture produced by Early Jurassic extension (e.g., Centamore et al., 1971). In such a framework, the Central Apennines developed during Miocene to Plio-Pleistocene times (e.g. Parotto and Praturlon, 1975; Barchi et al., 1998; Mazzoli et al., 2002; Bollati et al., 2012).

The Central Apennines involves the Umbria-Marche succession, which essentially includes Triassic to Miocene carbonates and marls, covered by Miocene to Pliocene syn-orogenic clastic sediments (Fig. 1). The pre-orogenic succession, from bottom to top, includes Late Triassic evaporites, dolomites and limestones ~~(~~of the Burano Formation~~),~~ which the basal detachment runs within its evaporitic interval (Ghisetti and Vezzani, 2000), Early to Late Jurassic platform and basinal limestones and dolostones (Calcare Massiccio, Corniola, Rosso Ammonitico, Calcari a Posidonia and Calcari ad Aptici Formations), and Cretaceous to Early Miocene basinal carbonates (Maiolica, Marne a Fucoidi, Scaglia and Biscaro Formations). In general, the lower part of the Burano Formation is overlaid by the fluvio-deltaic ~~siliciclastics~~ siliciclastic rocks of the Verrucano Formation (Middle-Late Triassic) (Tongiorgi et al., 1977; Ghisetti and Vezzani, 2000; Tavani et al., 2008). Nevertheless, the existence of these ~~siliciclastics~~ siliciclastic rocks in the Montagna dei Fiori area is not yet ~~proved~~proven. Syn-

orogenic deposits include Miocene marls and turbiditic sandstones (Marne con Cerrogna and Laga Formations) (Artoni, 2013 and references therein).

The deposition of the Calcare Massiccio Formation~~, (dated as~~ Hettangian-Sinemurian~~) and~~ with a total thickness varying between 300 to 700 m (Pialli, 1971), records an important extension pulse in the evolution of Tethyan rifting. The ~~following facies are observed in the~~ lower part of ~~the Calcare Massiccio Formation~~this formation which has been interpreted as having been deposited in a peritidal environment~~:~~ consists of ~~oncoid rich~~ peloidal pack- to grainstones in alternation with peloidal wacke- to packstones including horizons of algal bindstones (Calcare Massiccio A; Brandano et al., 2016). The upper part is made up of beds of skeletal and coated grain wacke- to grainstones ~~including microoncoids, echinoderms, calcareous and siliceous sponges, bivalves, gastropods and ammonites~~ (Calcare Massiccio B; Brandano et al., 2016). It ~~The lower part has been interpreted as having been deposited in a peritidal environment, while the upper part~~ corresponds to lower to middle shelf depositional environments, characterized by a general ~~deepening~~ deepening-upward trend ~~associated with extensional faulting and drowning of the platform, coupled with subsidence and deposition of the overlying Corniola Formation in the pelagic areas~~. Overall, the Early Jurassic rifting led to the growth of the Calcare Massiccio Formation in a carbonate platform setting, followed by faulting and drowning, and development of pelagic intrabasins filled by syn-rift sediments (Fig. 1c; Bernoulli et al. 1979; Santantonio and Carminati, 2011). The syn-rift sediments include pelagic limestones of the Bugarone and Corniola Formations. Condensed pelagic limestones of the Bugarone Formation (Lower Pliensbachian-Lower Tithonian; Bugarone Group in Pierantoni et al., 2013) occur at the top of the Calcare Massiccio Formation where it formed fault-controlled highs marking the regional drowning of the carbonate platform (Santantonio and Carminati, 2011). The pelagic limestones of the Corniola Formation (Sinemurian-Toarcian; Colacicchi et al., 1975; Morettini et al., 2002; Bosence et al., 2009; Marino and Santantonio, 2010; Brandano et al., 2016) occur within the fault-controlled (half)grabens in lateral continuation with the Calcare Massiccio Formation. The Corniola Formation in the lower part consists of turbiditic lobes which originated from tectonic brecciation of the Calcare Massiccio Formation. The upper part consists of a well-bedded pelagic mudstone with chert nodules (Di Francesco et al., 2010). ~~In the Montagna dei Fiori, the geologic framework of the outcropping Calcare Massiccio Formation is still a matter of debate between a~~

~~fault-related tectonosedimentary pattern (Mattei, 1987; Storti et al., 2017b), and a gravity-driven, olistolith hypothesis (Di Francesco et al, 2010; Santantonio et al., 2017). However, recent~~

2.1 Structural Framework

The Montagna dei Fiori Anticline is intersected by two major fault categories (Storti et al., 2018), which based on the chronological order include: ~~detailed work in the Salinello valley (Storti et al., 2017a; 2018)~~ Firstly, ~ E-W and ~ N-S striking fault zones showing extensional kinematics bounding the ~~documented that~~ major outcrops of Calcare Massiccio ~~are bounded by mostly ~ E-W and ~ N-S striking fault zones showing extensional kinematics~~ and dominantly affecting the Jurassic rocks older than the Maiolica Formation (Fig. ~~2A~~2a, e.g. sites 1 to 4). Overprinting relations indicate that ~ E-W deformation structures are systematically younger than the ~ N-S ones. Similar trends were observed in syn-rift fault zones in other anticlines of the Central Apennines (e.g. Cooper and Burbi, 1986; Alvarez, 1989; Chilovi et al., 2002). Such a tectonosedimentary inheritance was involved in the growth of the Montagna dei Fiori Anticline, which initiated during the Late Miocene (Mazzoli et al., 2002; Artoni, 2003) and progressively evolved into the upper thrust sheet of a well-developed antiformal stack until Plio-Pleistocene times (e.g. Ghisetti et al., 1993; Calamita et al., 1994; Artoni, 2013). The second set of faults is ~~A~~ a major structural feature trending parallel to the Montagna dei Fiori Anticline and dissecting it is the Montagna dei Fiori Fault, a NNW-SSE striking extensional fault system cutting at a high angle through the folded footwall rocks, typically at the forelimb-crest transition (Figs. 1, 2). This fault consists of two partially overlapping main fault zones with an extensional stratigraphic separation exceeding 900 m, and ~~This fault system~~ juxtaposes intensely deformed Late Miocene sediments in the hanging wall, against dolomitized and undolomitized Lower Jurassic and Cretaceous limestones in the footwall (Figs. 1 and 2). The development of the Montagna dei Fiori Fault has been alternatively interpreted as either a pre- (e.g. Calamita et al., 1994, Mazzoli, 2002; Scisciani et al., 2002) or late-folding (Ghisetti and Vezzani, 2000) feature. More recently, the origin of the Montagna dei Fiori Fault has been ascribed to the mutual interaction between horizontal shortening and uplift, and episodic gravitational re-equilibration during antiformal stacking underneath the anticline during Plio-Pleistocene times (Storti et al., 2018). The dolomitized intervals are exposed in the damage zones of the both aforementioned fault categories.

3 Methodology

The fieldwork covered an area of over 4 km^2 to delineate the distribution of dolostones. The stratigraphic and deformational features of dolostones were analyzed in more than 60 outcrops. The distribution of dolomitized intervals as well as their cross-cutting relationships with bedding planes, stylolites, veins and ~~structures~~ faults were ~~ground-truthed~~documented and sampled. For petrographic analyses, 130 polished thin sections were studied with standard petrographic methods (transmitted and UV-fluorescent light microscopy). Dolomite crystal morphology and texture is based on the classification proposed by Sibley and Gregg (1987).

The rock slabs and thin sections were stained using Alizarine Red S and potassium ferricyanide (Dickson, 1966) to discriminate dolomite from calcite and evaluate their iron content. Cold cathodoluminescence microscopy (CL) was carried out on representative thin sections (n = 80) at KU Leuven University (Belgium) using a Technosyn cathodoluminescence device (8-15 kV, 200-400 µA gun current, 0.05 Torr vacuum and 5 mm beam width).

$\delta^{13}C$ and $\delta^{18}O$ analysis were carried out on 117 samples. To ensure the sampling quality and avoid physical mixing of different diagenetic phases, the thin section images were mapped and the sampling targets were determined. Nevertheless, some diagenetic phases could not be isolated due to their sequential overgrowth and small size. Powder samples (150 - 200 µg) were obtained by applying a New Wave Research micromilling device and a dental drill at KU Leuven University (Belgium). The analysis was conducted at Parma University (Italy) and the Friedrich-Alexander-Universität (Erlangen-Nürnberg, Germany) laboratories using Finnigan DeltaPlus V and ThermoFinnigan 252 mass spectrometers, respectively. The carbonate powders were reacted with 100% phosphoric acid at constant temperature of 75°C. Several additional CO_2 reference gases (NBS18, NBS19, MAB99, and a pure Carrara marble) with known isotopic ratio were analyzed during the measurements to determine the $\delta^{13}C$ and $\delta^{18}O$ values of the sample. Reproducibility was checked by replicate analysis of laboratory standards and was better than ±0.1‰ for $\delta^{13}C$ and ±0.2‰ for $\delta^{18}O$ at Parma University and ±0.04 for $\delta^{13}C$ and ±0.05‰ for $\delta^{18}O$ at Friedrich-Alexander-Universität. Oxygen isotope composition of dolomites was corrected using the acid fractionation factors given by Rosenbaum and Sheppard (1986). Duplicate homogeneous samples measured in both labs for inter-laboratory reproducibility ~~show $\delta^{13}C$ and $\delta^{18}O$ values within the acceptable range of error deviation (±0.1‰) both for $\delta^{13}C$ and $\delta^{18}O$~~. All carbon and oxygen values are reported in per mil, relative to the "Vienna Pee Dee Belemnite~~Vienna PDB scale~~" (V-PDB).

A total number of 21 samples were analyzed for their $^{87}Sr/^{86}Sr$ ratios. The analyses were conducted at the Department of Analytical Chemistry, Ghent University (Belgium) and at the Vrije Universiteit Amsterdam (the Netherlands). NIST SRM 987 was used as the international Sr standard in both labs. At Ghent University, 15 sample powders (20 mg) were collected using a dental drill device. The $^{87}Sr/^{86}Sr$ ratio measurements were performed using a Thermo Scientific Neptune Multi-collector Inductively Coupled Plasma Mass Spectrometer (MC-ICP-MS) instrument. Within the external precision, repeated analyses of the international Sr standard yielded an average $^{87}Sr/^{86}Sr$ ratio of 0.710271 ± 0.000023 (2SD, n = 43), in agreement with the accepted $^{87}Sr/^{86}Sr$ ratio of 0.710248 for this reference sample (Thirlwall, 1991). At Vrije Universiteit Amsterdam, 6 sample powders (2 - 3 mg) were collected using a New Wave Research micromilling device. Analyses were performed using a ThermoElectron Triton plus TIMS instrument. In order to monitor and document the system's performance, repeated analyses of the international Sr standard (n = 58) were carried out on load sizes of 10 ng and 100 ng which yielded average $^{87}Sr/^{86}Sr$ ratios of 0.710245±0.000022 (2SD) and 0.710242±0.000008 (2SD), respectively. In both labs mass discrimination correction was performed via internal normalization using Russell's exponential law and the accepted value (0.1194; Steiger and Jager, 1977) of the invariant $^{86}Sr/^{88}Sr$ ratio.

Fluid inclusion microthermometry analysis was performed on 11 doubly polished wafers (80-130 µm in thickness). Measurements were carried out at Parma University (Italy) using Linkam THMSG-600 and Linkam MDS-600 heating-cooling stages coupled with a Leica DM 2500 microscope. The final melt (Tm_{ice}) and homogenization temperatures (T_h) were reproducible within 0.5°C and 5°C, respectively. The stages were calibrated by synthetic Syn Flinc™ fluid inclusion standards. A 100x objective was used during the microthermometry runs of the small inclusions. The microthermometry data were collected following the Fluid Inclusion Assemblage (FIA) approach described in Goldstein and Reynolds (1994) for carbonate minerals. The inconsistent homogenization temperatures and salinities obtained for these fluid inclusions, within the framework of an individual fluid inclusion assemblage (FIA) described by Goldstein and Reynolds (1994), indicate possible re-equilibration (stretched) of these inclusions and thus are not used in the interpretations. It is common for small inclusions (< 3 µm) to remain mono-phase all-liquid at room temperature due to their metastability (Goldstein and Reynolds, 1994). Thus, to eliminate the possible role of metastability, the samples were placed in a freezer for

several days following the procedures described in detail by Goldstein and Reynolds (1994). All-liquid inclusions remained unchanged and no vapor bubble was developed within them, which discards the metastability effect. In order to properly observe the phase transitions and determine the final melting temperature of ice in the all-liquid inclusions, they were rapidly heated up to ~ 200°C to stretch and nucleate a bubble at room temperature (Goldstein, 1990). The salinities are reported in equivalent weight percent NaCl (eq. wt. % NaCl) and were calculated based on the equation of Bodnar (1993). The homogenization temperatures obtained in all fluid inclusion assemblages indicate the minimum temperatures at which the fluids could have been trapped (Goldstein and Reynolds, 1994). No correction was made for pressure effects on entrapment temperatures since no data regarding the exact depth and pressure of entrapment are available. In absence of independent thermal indicators such as Conodont Alteration Index (CIA) and Vitrinite Reflectance (VR), the accuracy of pressure correction cannot be well constrained (Slobodník et al, 2006), and thus no correction was made for pressure effects on homogenization temperatures.

In order to perform ~~a~~ high resolution petrography, Scanning Electron Microscope (SEM) and Back-scattered Scanning Electron Microscope (BSEM) analyses were conducted using a Jeol 6400 Scanning Electron Microscope (SEM) equipped with an Oxford EDS (Energy Dispersive System). Operating conditions were 15 kV and 1.2 nA, electron beam about 1 μm in diameter and 100 s counting time; errors are ±2-5% for major elements and ±5-10% for minor components. The analysis focused mainly on detecting possible dolomite crystals inside the bed-perpendicular stylolites affecting the Cretaceous Scaglia Formation.

4 Results

4.1 Field observation and distribution of the dolomitized bodies

~~Dolomitization affected the Calcare Massiccio, Bugarone and Corniola Formations.~~ There is no evidence~~s~~ of dolomitization in the overlying and immediate surrounding successions of the Calcare Massiccio, Bugarone and Corniola Formations (e.g. Maiolica and Scaglia Formations), though the base of Maiolica Formation is reported as dolomitized in the Central Apennines onshore (e.g. Pierantoni et al., 2013) and offshore areas (Murgia et al., 2004).

Dolomitized intervals are folded in the forelimb of the Montagna dei Fiori Anticline and are abruptly truncated by the Montagna dei Fiori Fault, which juxtaposes them against intensely foliated Scaglia, Bisciaro and Marne con Cerrogna Formations (Figs. 2 and 3). The distribution

of dolomitized intervals is wider in the Salinello ~~valley~~ creek (Figs. ~~1B~~1b, ~~2A~~2a) perhaps due to a better exposure. In the Corano Quarry location, dolomitization occur in the Calcare Massiccio and Bugarone Formations only as meter-sized dolostone geobodies in the footwall of the Montagna dei Fiori Fault (Fig. 4). The map pattern (Fig. 2) of dolostones indicates that their distribution is maximized in the Castel Manfrino-Osso Caprino hill area and fades out both southward and eastward.

~~Dolostone breccias in fault cores is typically clast supported, with angular and millimeter- to centimeter-sized fragments (Fig. 3C), changing to crackle breccia (Woodcock and Mort, 2008) away from the master slip surface. In the proximity of the master slip surface, dolostone fragments are sporadically overprinted by millimeter-sized dolomite veins. The breccia fragments, where cemented, are commonly surrounded by calcite.~~

~~Dolomitization does not follow a systematic pattern.~~ The lateral extent of dolomitization is gradual. In some outcrops, dolomitization fronts show irregular outlines following, but also cross-cutting~~, the~~ bedding surfaces (Fig. 5). Dolomitized intervals vary in thickness from a few meters to hundred meters affecting the totality of the exposed Calcare Massiccio and ~~only~~ the lower part of Corniola Formation, where no clay interlayers are present. In the Calcare Massiccio Formation, dolomitization does not follow a systematic pattern. In the northern side of the Osso Caprino hill (Fig. 2), the top of formation is dolomitized but moving toward the Salinello creek, a thick non dolomitized limestone is exposed. The same situation occurs on the opposite side of the creek and to the east of Castel Manfrino.

Dolomitized intervals in the Corniola Formation have a darker color relative to the host rock and are systematically more fractured than the hosting limestone. High amplitude (> 1 mm), bed-parallel stylolites are clearly visible in both limestones and dolostones (Fig. 5). However, in some dolostones only ghosts of stylolite traces can be seen. No apparent porosity could be observed in host rock limestones but ~~The~~ the dolostones locally contain porosity, appearing as millimetre- to centimetre-sized pores. Dolostone breccias in fault cores are typically clast-supported, with angular and millimeter- to centimeter-sized fragments (Fig. 3C), changing to crackle breccia (Woodcock and Mort, 2008) away from the main slip surface. In the proximity of the main slip surface, dolostone fragments are sporadically cross-cut by millimeter-sized dolomite veins. The breccia fragments, where cemented, are commonly surrounded by calcite cement.

4.2 Petrography

4.2.1 Early calcite cementation

The early diagenetic products in the studied intervals are generally non-ferroan calcite cements. The first calcite cements precipitated following a phase of bioclast micritization (*sensu* Bathurst, 1975) in ~~grain-~~grain-supported intervals. In chronological order, they include: 1) fibrous cements (FC) riming the bioclasts, mostly in the peloidal facies of the Calcare Massiccio Formation (Fig. ~~6A~~6a). These cements are ~~dull~~ dark brown to non-luminescent under cathodoluminescence; 2) mosaic cements (MC), commonly fill the intergranular pore spaces (Fig. ~~6B~~6b), and also occur as syntaxial overgrowths on echinoderm fragments. ~~These cements~~They exhibit deformation twinning and show a well-developed ~~dull~~ brown and orange concentrically-zoned cathodoluminescence pattern (Figs. ~~6C~~ 6c and ~~D~~d). They contain only mono-phase all-liquid inclusions. All of these cements are postdated by dolomites and high amplitude bed-parallel stylolites (Fig. 6b).

4.2.2 Dolomitization

All the dolomite types are non-ferroan and dominantly fabric destructive. Dolomitization developed in all the facies types of the Calcare Massiccio and the overlaying Bugarone Formations, but only at the lower part of the Corniola Formation which consists of resedimented Calcare Massiccio breccias (turbiditic lobes).

The two first dolomite types (D1 and D2) are the dominant dolomite types in the studied outcrops. These dolomites are distributed within the damage zones of the ~ N-S and E-W Jurassic rift-related extensional faults and, in places, displaced by them (Fig. ~~2A~~2a, site 1). The third and fourth dolomite types (D3 and D4) are mainly observed within the damage zone of the Montagna dei Fiori Fault (NNW-SSE), and appear only as dolomitic pockets locally replacing the host rock and ~~overprinting~~ overgrowing D1 and D2 at the proximity of the ~ N-S and E-W extensional faults. The fifth dolomite type (D5) is found only within the brecciated zones associated with the Montagna dei Fiori Fault damage zone. The distinctive petrographic features of the recognized dolomite types are summarized below:

Dolomite 1 (D1) is a replacive dolomite which commonly appears as dispersed rhombs and aggregates, and locally rims fracture walls cemented by calcite ~~(CV1)~~ (Figs. ~~6E~~ 6e and ~~F~~f). D1 postdates the micritic envelopes and early calcite cements, and predates high amplitude bed-parallel stylolites (Figs. ~~6G~~ 6g and ~~H~~h). The crystals are fine to medium sized (< 350 µm) ~~and~~

with planar-e and planar-s textures, ~~consists~~ consisting of relatively turbid, rich in host rock solid-inclusions~~ rich~~, well-developed ~~euhedral to subhedral~~ crystals~~,~~. They show ~~with~~ red luminescence when viewed under cathodoluminescence~~, occasionally developing a concentrical zonation~~.

Dolomite 2 (D2) is a replacive dolomite (Figs. ~~7A~~ 7a and ~~B~~b), infrequently occluding existing pore spaces. Like D1, it also ~~frequently~~ predates high amplitude bed-parallel stylolites (Figs. ~~6G~~ 6g and ~~H~~h). D2 generally exhibits a ~~tightly~~ closely packed texture with no or little intercrystalline porosity. The crystals are medium to coarse sized (≤ 500 µm) with planar-s to non-planar textures. They includ~~e~~ing a turbid core followed by a transparent ~~subhedral to anhedral~~ rim and trace quantities of saddle dolomite developing ~~swiping~~ sweeping extinction. In some crystals, one additional turbid zone rich in host rock solid inclusions and fluid inclusions of mostly mono-phase is present. Cathodoluminescence observations enabled to recognize the presence of D1 in their turbid cores. D2 crystals are characterized by zones of bright red-pink luminescence separated by purple luminescence zones (Fig. 7b).

Dolomite 3 (D3) is present as small localized bodies in the Calcare Massiccio (at the Castel Manfrino reference section), in the Corniola Formation (at the Osso Caprino Road), and in the Calcare Massiccio and Bugarone Formations (at the Corano Quarry) (Figs. 1b and 2a). In the Corano Quarry the dolomitized Bugarone and Calcare Massiccio Formations are in the footwall of the Montagna dei Fiori Fault; and juxtaposed to the ~~undolomitezed~~undolomitized, intensely foliated Scaglia Formation in ~~(~~the hanging wall~~)~~. The SEM and BSEM analysis performed on the samples from the immediate adjacent Scaglia Formation within the aforementioned fault damage zone did not indicate the presence of any dolomite in this formation. Within the Bugarone Formation in this fault damage zone, D3 locally cements the millimeter-sized angular breccias that are in turn affected by ~~fault~~ fault-parallel stylolites (Figs. ~~7C~~ 7c and ~~D~~d). ~~The SEM and BSEM analysis performed on the samples from the immediate adjacent Scaglia Formation within the aforementioned fault damage zone did not indicate the presence of any dolomite in this formation.~~ D3 crystals are fine to medium sized (< 300 µm) ~~mostly transparent euhedral to anhedral~~exhibiting planar-e to non-planar textures ~~(< 300 µm)~~, with minor development of saddle morphologies ~~in~~ of larger crystals (> 500 µm) with planar-c texture (Figs. ~~7E~~ 7e to ~~H~~h). The ~~euhedral to anhedral~~replacive crystals ~~are generally replacive,~~ display~~ing~~ a faint core, which compared to previous dolomite types has fewer solid inclusions. The saddle crystals are

occasionally replacive ~~but majorly appear as cement in fractures~~. They display typical curved and slightly serrated crystal terminations with ~~swiping~~ sweeping extinction. These saddle dolomites were only observed in the Castel Manfrino reference section. D3 generally exhibit a ~~dull~~ dark purple color with bright orange zones and subzones in core and/or rims when viewed under cathodoluminescence (Figs. ~~7E~~ 7e to ~~H~~h).

Dolomite 4 (D4) appears as a matrix replacive and dolomite cement surrounding porosity, and locally ~~recrystallizing~~ replacing D1 and D2 (Figs. ~~8A~~ 8a to ~~F~~f). D4 also occludes ~~bed~~ bed-parallel shear fractures and appears along the ~~bed~~ bed-parallel stylolites (Figs. ~~9A~~ 9a to ~~D~~d). In the Castel Manfrino reference section, some intercrystalline vuggy porosity is filled with fine dolomite rhombs including D4 with relics of D2 within their core (Figs. ~~8E~~ 8e and ~~F~~f). ~~The~~ This porosity may be preserved or partially to completely filled by calcite (~~CV4~~C4). D4 crystals have a turbid, solid-inclusion rich core and transparent rim. They are fine to medium sized (< 200-350 µm), presenting ~~subhedral~~ planar-s ~~to~~ and infrequent ~~euhedral crystals~~non-planar textures. D4 exhibits a distinct luminescence pattern including a purple zone and an irregular green subzone.

Dolomite 5 (D5) occurs as crystals cementing micro-veins that cross-cut precursor dolomite types including dolomitic breccia fragments. In cemented breccias, D5 is postdated by ~~CV3~~C3. D5 presents a planar-c texture ~~is transparent, anhedral~~ and is characterized by a bright red luminescence (Figs. ~~9E~~ 9e and ~~F~~f).

4.2.3 Late calcite cementation

Four generations of calcite ~~veins~~ postdating dolomitization and distributed only within the fault damage zones have been identified (Figs. 10 and 11):

~~1)~~ Calcite ~~vein~~ 1 (C~~V~~1) occurs only in Calcare Massicio limestones and dolostones and is represented as centimeter-sized veins with thickness that does not exceed 1.5 cm. It is not clear whether the fracture opening and calcite precipitation was simultaneous (as shown in Ukar and Laubach, 2016). These veins are strata-bound, bed~~ding~~-perpendicular ~~veins~~ with irregular fracture walls, exhibiting white color in the outcrops. They are present within the syn-rift related extensional fault damage zones, ~~postdate~~postdating the first dolomite type (D1) and abutted ~~riming the same fractures that abut the high~~by high amplitude ~~bed~~ bed-parallel stylolites. C~~V~~1 ~~often~~ usually shows blocky to elongated crystal morphologies and displays well-developed deformation twinning planes (Type II of Burkhard, 1993). This calcite exhibits concentric~~al~~

zonation and ~~dull~~ brown zones alternate with orange luminescence zones (Figs. ~~11A~~ 11a and ~~B~~b).

~~2)~~ Calcite ~~vein~~ 2 (C~~V~~2) exclusively occurs in the intensely deformed Scaglia Formation within the fault damage zones (Figs. 11b, c and d) and correspond to tension gashes associated with stylolites (*sensu* Nelson, 1981). The thickness of these veins does exceed 1 cm. They are usually discontinuous and branch to several microveins (thickness < 1mm) when their tips are not intersected by stylolites. ~~CV2~~C2 veins are mostly recorded in foliated shear deformation zones with well-defined S-C fabrics, exhibiting blocky, elongated to fibrous shapes with strongly developed tightly spaced deformation twinning planes (Type II of Burkhard, 1993). ~~CV2~~C2 displays ~~yellow~~ brown to orange luminescence with locally darker sector zones. The ~~yellow~~ brown to orange luminescence characteristic of ~~CV2~~C2 is ~~comparable with~~similar to those of encasing Scaglia host rocks (Figs. ~~11C~~ 11c and ~~D~~d).

~~3)~~ Calcite ~~vein~~ 3 (C~~C1~~C1~~V~~3) occurs as cement, filling the ~~extensional faults~~Montagna dei Fiori ~~master~~ main fault plane and isolated veins within ~~the extesional fault~~its damage zone~~s~~. These veins are centimeter-sized with thicknesses of less than 2 cm. The breccias are generally clast-supported, but locally ~~CV3~~C3 cements the brecciated fault-infillings containing angular fragments of host rock limestones, dolostones and earlier calcites. In the brecciated zones ~~at the backlimb of the anticline (Montagna dei Fiori Fault)~~, ~~CV3~~C3 always passively overgrows D5 in fractures and never cuts it.~~postdates the last dolomitization phase (D5) with no evidence of physical disruption.~~ ~~CV3~~C3 exhibits a translucent white ~~to translucent~~ color in hand specimen. The crystals are blocky with no or weakly developed deformation twinning planes, and are characterized by a dark orange to brown luminescence with distinct darker sector zones (Figs. ~~11E~~ 11e and ~~F~~f).

~~4)~~ Calcite vein 4 (~~CV4~~C4) exists as centimeter-sized isolated veins, pore-filling as well as breccia cements postdating all the preceding dolomites and calcites in the Montagna dei Fiori main fault plane. The breccia fragments are ~~more often~~usually dolostones. ~~CV4~~C4 has a translucent white ~~to translucent white~~ color in hand specimen with blocky crystal morphology and no evidence of subsequent deformation (e.g. deformation twinning planes), and is characterized by distinct concentric~~al~~ zonation (Figs. ~~11G~~ 11g and ~~H~~h).

4.3 Geochemistry

4.3.1 Carbon and oxygen stable isotopes

The carbon and oxygen stable isotopic data ($\delta^{13}C$ and $\delta^{18}O$) of host rocks, dolomites and calcites are given in Table 1 and shown in Figures ~~12A~~ 12a and ~~B~~b. The marine stable isotopic compositions reported by Veizer et al. (1999) were used as marine reference values. Accordingly, Lower Jurassic marine limestones are characterized by $\delta^{13}C$ values of -0.5 to +4.5‰ and $\delta^{18}O$ values of -2.5 to +1.0‰ V-PDB. The $\delta^{18}O$ values of the marine dolomites are known to be 3-4‰ V-PDB more enriched than those of co-genetic marine limestones (Land, 1980; Major et al., 1992; Horita, 2014). In order to avoid data ambiguity due to physical mixing, this analysis was not separately performed on early calcite cements (FC and MC). The $\delta^{13}C$ and $\delta^{18}O$ values measured on bulk samples of host rock limestones. Both $\delta^{13}C$ and $\delta^{18}O$ values of the host rocks are within the expected range of the Lower Jurassic marine limestones but the Corniola host rocks show slightly lower values comparing to those of Calcare Massiccio. In the Calcare Massiccio host rocks, the $\delta^{13}C$ values plot between +2.4 and +3.1‰ and $\delta^{18}O$ values are within the range of -1.6 and 0.0‰ V-PDB. The $\delta^{13}C$ values in the Corniola host rocks are +2.0 and +2.5‰ while the $\delta^{18}O$ values are -3.1 to -1.4‰ V-PDB. The $\delta^{13}C$ and $\delta^{18}O$ values of the Scaglia host rocks range between +1.0 to +3.3‰ for $\delta^{13}C$ and -2.2 to -1.0‰ V-PDB for $\delta^{18}O$. The ~~obtained~~ values obtained are characterized in the mean range of Upper Cretaceous to Paleogene marine limestones (Veizer et al., 1999; +1.0 to +4.5‰ for $\delta^{13}C$ and -4.0 to +2.0‰ V-PDB for $\delta^{18}O$).

The $\delta^{13}C$ values of ~~CV1~~C1 are between +1.6 and +2.1‰ which plot within the range of reference values (Jurassic) but are slightly lower than the surrounding host rock values. The $\delta^{18}O$ values are between -4.7 and -2.7‰ V-PDB which are lower than those of reference and host rock values.

The $\delta^{13}C$ values of all dolomite types (+0.6 to +3.4‰) fall within the range of host rocks and Jurassic marine limestones (Veizer et al., 1999). The $\delta^{18}O$ shows a wider range of values, ~~somehow~~ overlapping but also lower than ~~those of~~ host rocks (-4.5 to -0.9‰ V-PDB) and those expected for the ~~presumable~~ Lower Jurassic marine dolomites. The majority of values plot between -3.5 and -1.5‰ V-PDB. The small size and overgrowth nature of certain dolomite types (e.g. D2 and D5) limits their proper isolation for geochemical analyses. Only one sample from D1 dolomite could be measured for $\delta^{13}C$ and $\delta^{18}O$ values, showing +2.5 and -1.9‰ V-PDB, respectively. The $\delta^{13}C$ and $\delta^{18}O$ values of D3 dolomite range from +2.0 to +2.6‰ and -2.8 to -1.9‰ V-PDB, respectively, with values lower than those of the host rock.

D4 dolomite has $\delta^{13}C$ values between +2.4 and +2.5‰, and $\delta^{18}O$ values of -3.0 to -2.5‰ V-PDB. The $\delta^{13}C$ and $\delta^{18}O$ values of ~~CV2~~C2 are +1.2 to +3.1‰ and -1.7 to -1.7‰ V-PDB, respectively. The $\delta^{13}C$ values of ~~CV3~~C3 are between +0.5 and +2.4‰, and the $\delta^{18}O$ values cover a range of -2.2 to 0.0‰ V-PDB. The $\delta^{13}C$ and $\delta^{18}O$ values of ~~CV4~~C4 are +3.8 to +4.9‰ and -9.4 to -9.1‰ V-PDB, respectively. The $\delta^{13}C$ values are slightly higher but the $\delta^{18}O$ values are considerably lower compared to preceding calcite generations and the measured values from host rocks.

4.3.2 $^{87}Sr/^{86}Sr$ ratios

Samples from host rocks (i.e. Calcare Massiccio and Corniola Formations), dolomites (D1, D3 and D4) and the Scaglia Formation in juxtaposition with the dolostones were analyzed for their $^{87}Sr/^{86}Sr$ isotopic ratios. The obtained ratios versus $\delta^{18}O$ values of the analyzed samples are shown in Fig. 12C. The $^{87}Sr/^{86}Sr$ ratios obtained from the Calcare Massiccio and Corniola limestones are 0.70766 and 0.70725 (n = 2), respectively, which is in agreement with the values of the Lower Jurassic marine carbonates (0.70704-0.70768) reported by McArthur et al. (2012). CV1 show a value equal to 0.70773.

All the dolomite types display higher $^{87}Sr/^{86}Sr$ ratios when compared to the host rocks and reference values of the Lower Jurassic marine carbonates. D1 (replacive) and D4 cements show a ~~comparable~~ similar narrow range with values between 0.70784 and 0.70790, respectively. ~~While, the~~ The two D3 samples (replacive and cement) display higher $^{87}Sr/^{86}Sr$ ratios (0.70858 and 0.70963, respectively). The $^{87}Sr/^{86}Sr$ ratios obtained for dolomites do not show co-variation with corresponding $\delta^{18}O$ values. The radiogenic Sr analysis was not performed on D2 and D5 since the physical mixing with other dolomite types could not be avoided.

The $^{87}Sr/^{86}Sr$ ratios of the ~~two~~ three marly limestone samples of Scaglia Formation are 0.70784 to 0.70790. The ~~CV2~~C2 veins in Scaglia Formation show ~~comparable~~ similar ratios of 0.70779 and 0.70787. These values fit within the limits of values assigned by McArthur et al. (2012) for the Cenomanian-Bartonian (Scaglia age) marine carbonates (0.70730-0.70790).

4.4 Fluid inclusion microthermometry

The overview of microthermometry measurements is given in Table 1 and Figs. 13A to C. All the measured fluid inclusions are primary and occur in growth zones. Based on optical and fluorescence microscopy analysis of wafers all the inclusions are aqueous mono-phase (liquid)

and two-phase (liquid and vapor) with relatively consistent L:V ratio of 10-15% within a single FIA (fluid inclusion assemblage). Special care was taken to avoid the samples that occasionally displayed scattered mottled luminescence that may indicate recrystallization.

~~On the basis of optical microscopy analysis of wafers,~~ D1 contain dominantly mono-phase aqueous inclusions with sizes greater than 5 µm. ~~It is common for small inclusions (< 3 µm) to remain mono-phase all liquid at room temperature due to their metastability (Goldstein and Reynolds, 1994). Thus, to eliminate the possible role of metastability, the samples were placed in a freezer for several days following the procedures described in detail by Goldstein and Reynolds (1994). All liquid inclusions remained unchanged and no vapor bubble was developed within them, which discards the metastability effect. In order to properly observe the phase transitions in the all liquid inclusions, they were rapidly heated up to ~ 200°C to stretch and nucleate a bubble at room temperature (Goldstein, 1990).~~ All the inclusions froze at -65 to -49°C. The first melting (Te) was detected between -22 to -19.3°C. The final ice melting (Tm) appeared at temperatures between -7.7 and -2°C. Applying Bodnar´s (1993) equation, the obtained final melting temperatures correspond to salinity ranges of 3.5 to 11.3 eq. wt. % NaCl.

D2 is characterized by the presence of mono-phase and infrequent two-phase inclusions generally within their growth zones. The homogenization temperature of two-phase inclusions varies between 58 and 71°C. Upon cooling, a complete freezing of the fluid phase is reached at -56 to -40°C. The first ice melting temperature was distinguished at -22°C. The final ice melting temperatures fall within -17.5 and -5°C, corresponding to salinities between 7.9 and 20.5 eq. wt. % NaCl.

D3 is commonly inclusion poor. The measureable inclusions were detected and examined only in saddle dolomite crystals. These crystals contain only two-phase aqueous inclusions. Their homogenization temperatures are within the narrow range of 70 to 73°C. The complete freezing and first ice melting temperatures could not be distinguished but the final ice melting temperature occurred at temperatures between -13 and -6°C equal to salinity ranges of 9.2 to 16.9 eq. wt.% NaCl. The first melting temperatures of fluid inclusions in D1, D2 and D3 were about -21°C, suggesting a H_2O-NaCl fluid system.

D4 contains only two-phase aqueous inclusions. The homogenization temperatures in D4 vary between 79 and 105°C. Complete freezing of inclusions occurred at temperatures between -86 and -54 °C. The first ice melting was detected at -35 to -40°C indicating the

possible presence of divalent cations such as Ca^{2+} and/or Mg^{2+} in the fluids (Shepherd et al., 1985; Goldstein and Reynolds, 1994). The final ice melting temperatures fall within a range of -15 and -9°C corresponding to salinities of 12.8 to 18.6 eq. wt. % NaCl. A couple of inclusions show homogenization temperatures exceeding 120°C with salinities higher than 20 eq. wt. % NaCl. ~~The inconsistent homogenization temperatures and salinities obtained for these fluid inclusions, within the framework of an individual fluid inclusion assemblage (FIA) described by Goldstein and Reynolds (1994), indicate possible re-equilibration of these inclusions and thus are not used in the interpretations.~~

~~The obtained homogenization temperatures in all fluid inclusion assemblages indicate the minimum temperatures at which the fluids could have been trapped (Goldstein and Reynolds, 1994). No correction was made for pressure effects on entrapment temperatures since no data regarding the exact depth and pressure of entrapment are available. In absence of independent thermal indicators such as Conodont Alteration Index (CIA) and Vitrinite Reflectance (VR), the accuracy of pressure correction cannot be well constrained (Slobodník et al, 2006), and thus no correction was made for pressure effects on homogenization temperatures.~~

No measurable fluid inclusion could be identified in ~~CV1~~C1 and ~~CV2~~C2 due to intense deformation twinning. ~~CV3~~C3 and ~~CV4~~C4 contain only primary mono-phase aqueous inclusions, indicating an entrapment temperature of below about 40-50°C (Goldstein and Reynolds, 1994). A complete freezing of the inclusions in ~~CV3~~C3 occurred at temperatures between -40 and -52.5°C. The first melting temperature was detected at about -21 to -22°C, suggesting a H_2O-NaCl composition. The final melting temperatures range between -6.4 and -2.7°C, corresponding to salinities between 9.7 and 4.5 eq. wt. % NaCl. The majority of the values cluster between 7.8 and 5 eq. wt. % NaCl.

The complete freezing temperatures of the inclusions in ~~CV4~~C4 fall within -46 and -35.5°C. The first melting temperature could not be determined with confidence but the final melting temperatures were reached at about -0.1 to -1.8°C, corresponding to salinities of 0.17 to 3.0 eq. wt. % NaCl.

5 Discussion

5.1 Stable and radiogenic isotopic composition of the parental fluids

The $\delta^{13}C$ values of all dolomite types mimic the range of host rock and Jurassic marine limestones and, consequently, they can be interpreted as largely rock-buffered. Their $\delta^{18}O$ values

are partly ~~comparable~~ similar to those of their respective host rocks as well as Jurassic marine reference values but more depleted when compared to the presumable Jurassic marine dolomites. The relatively depleted $\delta^{18}O_{dolomite}$ values could indicate the contribution of heated fluids in dolomitization process, although it could also relate to recrystallization of a precursor dolomite by fluids at higher temperature or ^{18}O-depleted (Land, 1980; 1985). The absence of distinctive textural evidence in the analyzed samples such as enlarged crystal size and/or systematic mottled cathodoluminescence pattern, and their co-variation with $\delta^{18}O$ values do not confirm recrystallization (Mazzullo, 1992 and ref. therein). ~~Nevertheless, special care was taken to avoid the samples that occasionally displayed scattered mottled luminescence.~~

The oxygen isotope fractionation relation between water and dolomite (Land, 1983) was used to determine the most plausible parental fluids. In order to avoid erroneous results due to rock-buffered $\delta^{18}O$ values, only the $\delta^{18}O$ values of dolomite cements, especially from the ~~bed~~ bed-parallel veins containing D4 were used. These values may provide the closest approximation to the $\delta^{18}O$ signature of the parental fluids (Barker and Cox, 2011). Accordingly, a $\delta^{18}O$ value of ≈ +2.5 to +4‰ V-SMOW was calculated for D3, while this values increase to ≈ +5 to +7.5‰ V-SMOW for D4 (Fig. ~~13D~~13d). ~~The calculated compositions of the potential parental fluids are progressively higher~~ The higher $\delta^{18}O$ composition of the dolomitizing fluids relative to the Mesozoic seawater, which is estimated at -1.2 to -1‰ V-SMOW (Shackleton and Kennett, 1975; Marshall, 1992; Saelen et al., 1996), is compatible with fluids derived from or that had interacted with ~~siliciclastics~~siliciclastic rocks, crystalline basement (Taylor, 1997) and/or evaporite-derived brines.

The $^{87}Sr/^{86}Sr$ ratios obtained for all dolomite types are higher than the Lower Jurassic marine carbonate values (0.70704-0.70768; McArthur et al., 2012). Since marine carbonates have very low rubidium (Rb) concentrations they produce negligible *in situ* radiogenic ^{87}Sr after their deposition (Stueber et al. 1972; Burke et al. 1982). Therefore, the higher $^{87}Sr/^{86}Sr$ ratios can be explained by the contribution of fluids originated or interacted with potassium rich ~~siliciclastics~~ siliciclastic rocks (K-feldspars), crystalline basement and/or stratigraphic levels with higher $^{87}Sr/^{86}Sr$ ratios (Emery and Robinson 1993; Banner, 2004). Taking into account that the Upper Triassic Burano Formation underlying the studied intervals as the basal detachment has $^{87}Sr/^{86}Sr$ ratios between 0.70774 and 0.70794 (Boschetti et al., 2005), the $^{87}Sr/^{86}Sr$ ratios (D1 and D4) can partially be explained by their contribution. However, this contribution cannot justify

much higher $^{87}Sr/^{86}Sr$ ratios recorded in D3, being higher than values reported for Phanerozoic seawater (McArthur et al., 2012), and the values ~~recorded in~~obtained for the adjacent basinal deposits (i.e. Corniola and Scaglia Formations). Therefore, parental fluids most likely originated from or had interacted with the ~~siliciclastics~~ siliciclastic rocks underlying the Burano Formation (Verrucano Formation), if present, and/or with the crystalline basement with common elevated $^{87}Sr/^{86}Sr$ ratios (0.71500-0.72650; Del Moro et al., 1982). The significantly higher $^{87}Sr/^{86}Sr$ ratios in D3 in comparison with other studied dolomites indicates a higher influence of $^{87}Sr/^{86}Sr$-rich fluids either due to major changes in the permeability architecture of faults or availability of such fluids. The lack of any ferroan diagenetic phase minimizes the interaction of fluids produced by clay transformation/dewatering (i.e. smectite to illite transformation; Boles and Franks, 1979).

~~CV1~~C1 is characterized by $\delta^{13}C$ and $\delta^{18}O$ values lower than the host limestones (i.e. Calcare Massiccio), while its $^{87}Sr/^{86}Sr$ ratio is ~~comparable~~ similar to them. The salinity and composition of the parental fluids cannot be inferred here since no measurable fluid inclusions were found within this cement. The $^{87}Sr/^{86}Sr$ ratio being within the range of the corresponding host rocks and the reference values, points to a rock-buffered system for $^{87}Sr/^{86}Sr$.

The $\delta^{13}C$ and $\delta^{18}O$ values obtained for ~~CV2~~C2, as well as $^{87}Sr/^{86}Sr$ ratios, fall within the range of the Scaglia host rocks, thus reflecting their rock-buffered nature. This interpretation is further supported by the ~~comparable~~ similar luminescence characteristics of ~~CV2~~C2 with that of encasing Scaglia host rocks. The fluids from which ~~CV2~~C2 calcite precipitated, as expected for tension gashes, were most likely derived from carbonate dissolution during pressure-solution and stylolitization of host rock~~.~~, pointing to a closed fluid system in contrast with the subsequent vein generations.

~~CV3~~C3 is characterized by $\delta^{13}C$ values within the Jurassic marine values but are generally lower than the host rocks, while their $\delta^{18}O$ values partially overlap both the hosting limestones and dolostones. Microthermometry of fluid inclusions revealed only mono-phase aqueous inclusions and thus precipitation at relatively low temperature ($\leq$ 40-50°C) with moderate salinity (4.5-9.7 eq. wt. % NaCl). Such levels of salinity can be assigned to evaporated seawater, residual brines or fluids derived from evaporite dissolution, and thus makes it difficult here to interpret their exact origin with the available data.

~~CV4~~C4 is the latest calcite phase, and records the $\delta^{13}C$ and $\delta^{18}O$ values, respectively enriched and significantly depleted when compared to their hosting rocks and preceding

diagenetic products. Generally, the enrichment of ^{13}C could suggest CO_2 outgassing due to evaporation or pressure changes (Friedman, 1970; Hendry et al., 2015) or bacterial fermentation (methanogenesis) of organic matter (Hudson, 1977) in low temperature diagenetic environments. The homogenization temperature of ~~CV4~~C4, being below about 40-50°C, could support any of these processes. Their low $\delta^{18}O$ values and fluid inclusions with salinities ~~comparable~~ similar to, but also significantly lower than, seawater reflect the contribution of meteoric fluids during precipitation of this calcite.

5.2 Origin of the dolomitizing fluids

The contribution of brines that derived from highly evaporated seawater or evaporites is suggested by the elevated salinity values obtained from microthermometry of the fluid inclusions (3.5 to 20.5 eq. wt. % NaCl). Accordingly, two sources that could potentially provide such fluids can be proposed: 1) fluids related to the Late Messinian evaporites, associated with the overlying Upper Miocene Laga Formation, ~~deposited during the Upper Miocene time,~~ and their possible downward percolation through fault zones by density driven flow and/or seismic pumping mechanisms (Sibson, 1981; McCaig, 1988, 1990); or their tectonic involvement into the Apenninic thrust wedge during its propagation (underthrusting; Lobato et al., 1983); and 2) fluids related to the underlying ~~décollement~~ detachment horizon of the Burano evaporites (Upper Triassic) and their upward flow through fault zones during development of the Montagna dei Fiori Anticline. The first scenario is valid if the dolomitization would have occurred only from the Upper Miocene time onwards. Moreover, ~~Several~~ several researchers (e.g. Vai and Ricci Lucchi, 1977; Bassetti et al., 1998; Roveri et al. 2001) have shown that the occurrence of primary shallow-water evaporites, which were dominantly gypsum, was limited only to the western and central parts of the northern Apennines consisting of thrust-top marginal basins~~. In contrast, evaporites never precipitated in parts of the central Apennines including the Montagna dei Fiori region (Marche area)~~ (Roveri et al. 2001). Hence, the evaporitic horizons existing within the Laga Formation corresponds to resedimentation (gypsum debris) of those previously precipitated in the marginal basins. This interpretation makes the Messinian evaporites an unlikely source of Mg-rich brines. ~~Moreover, taking~~ Taking into account that the maximum ~~burial~~ burial-related temperature of the Calcare Massiccio Formation did not exceed 80°C in the Montagna dei Fiori region (Ronchi et al., 2003), ~~it's~~ it is ~~not~~ unlikely that the downward percolation of relatively low-temperature brines derived from the Messinian evaporites, located

at ~~the~~ higher stratigraphic levels, could reach or exceed the high temperatures recorded in fluid inclusions of the studied dolomites ~~in the Calcare Massiccio Formation~~ (D4; up to 105°C), given that the homogenization temperatures reflect the minimum entrapment temperatures (Goldstein and Reynolds, 1994). Deep circulation of these brines, if they existed, can also be excluded by the fact that their limited ~~tectonic~~ involvement ~~with~~in the thrust wedge ~~being~~ was confined merely to the off shore wards of the Montagna dei Fiori region (Artoni, 2013).

Accordingly, the Upper Triassic Burano Formation, the basal detachment, appears as the most plausible source for the high salinity brines recorded in fluid inclusions, and likewise, the Mg-rich fluids could have been originated from post-evaporite brines associated with them (Carpenter, 1978; McCaffrey et al., 1987). The fluctuations in salinity may argue for ~~different degrees of~~ diverse range of fault connectivity, different degrees of rock-water interaction and contribution of pore waters of lower salinity (e.g. marine or meteoric).

5.3 Timing and structural controls on the evolution of parental fluids

A generalized paragenesis and the relative chronology of dolomitization in relation to the structural evolution of the Montagna dei Fiori Anticline are illustrated in Figs. 14 and 15. The structural episodes are based on the evolutionary stages of the Montagna dei Fiori Anticline suggested by Storti et al. (2018). The paragenesis is constructed on the basis of direct evidences recorded during observations at outcrop scale and microscopic observations (e.g. cross-cutting relationships between diagenetic phases, stylolites, fractures and other structural kinematics), and indirect evidences (e.g. regional geodynamics and burial history).

The occurrence of micritic envelopes and fibrous calcite cements (FC), in ~~grain~~ grain-supported stratigraphic levels of the Calcare Massiccio Formation, is interpreted to be of eogenetic origin (i.e. marine phreatic diagenesis; Moore, 1989), reflecting an early diagenesis shortly after deposition. The well-developed ~~dull~~ brown and orange concentric cathodoluminescence pattern of the succeeding mosaic calcite cement (MC) suggests a progressive shift to more reducing conditions during precipitation in a phreatic diagenetic environment (as shown in Li et al., 2017). High amplitude ~~bed~~ bed-parallel stylolites postdate both cements, which confirm their precipitation before significant burial. The observations made here are in agreement with earlier work by Giacometti and Ronchi (2000), interpreting that the Calcare Massiccio Formation was cemented during the early diagenetic stages.

D1, ~~CV1~~C1 and D2 are ~~postdated~~ cut by well-developed, high amplitude bed-parallel stylolites. Presence of D1 and ~~CV1~~C1 in bed-perpendicular veins typically ~~abutted~~ cut by these stylolites (see Figs. ~~6E~~ 6e to ~~H~~h) support the interpretation that the first dolomitization event (D1 and D2) took place before significant burial and stylolite development~~, .~~ ~~being t~~The latter and bed-perpendicular veins are dynamically compatible within the same stress field which is characterized by a vertical, load-related maximum principal axis of the stress ellipsoid (Fig. 15a). The dominantly mono-phase fluid inclusions within D1 and D2 are in agreement with precipitation temperatures below about 40-50°C, suggesting a relatively shallow to intermediate burial environment and hence supporting a pre-Apenninic orogeny age of precipitation from a mix of formational and extra-formational fluids with elevated $^{87}Sr/^{86}Sr$ ratios. The distribution of D1 and D2 localized nearby the rifting-related ~ N-S and E-W striking extensional faults and even their displacement along them (Fig. ~~2A~~2a, e.g. site 1), point to the possible contribution of these faults in occurrence of D1 and D2. These faults dominantly affect the Jurassic rocks older than the Maiolica Formation which is attributed to ~~the~~ post-rift deposits, therefore suggesting a pre-Maiolica age for these dolomite types. Although~~,~~ an absolute age cannot be provided, based on the evidence discussed above, the circulation of Mg-rich fluids during this dolomitization event was most likely controlled by rifting-related Jurassic extensional fault zones cutting through the crystalline basement. Precipitation of D1 and D2 at the lower part of Corniola Formation which is known as the syn-rift deposit discards a pre-rift origin for these dolomites. The displacement of dolomites along the aforementioned faults is possibly related to their prolonged activation during Early to Late Jurassic. In addition to the role of these faults in channelizing the fluids, their mobilization must have been intensified by some deriving mechanisms. A thermal convection system derived from high hit flux during rifting was interpreted by Hollis et al. (2017) to be responsible for circulation of seawater in a syn-rift dolomitization case in the Hammam Faraun fault block (Suez Rift, Egypt). In such scenario, the salinity of the fluids and their $^{87}Sr/^{86}Sr$ ratios are expected to be more or less within the range of seawater. Furthermore, this scenario seems unlikely in the studied area given the lack of a deep aquifer to accommodate the fault tips and promotes the lateral fluid flux from basin to the rift shoulders and vice versa. Taking into account that D1 and D2 are the volumetrically more relevant dolomites within the studied intervals, and assuming the likely role of syn-rift extensional faults (Early to Late Jurassic) in their precipitation, a dominantly syn-rift

dolomitization process is proposed for the dolostones in the Montagna dei Fiori Anticline. Although the CL zonation pattern observed in D2 may indicate changes in flow condition or fluid composition, the lack of physical disruptions such as multiple fracturing suggests external regional controls rather than slip along the same faults (Eichhubl and Boles, 2000). The absence of pervasive syn-dolomitization fracturing and brecciation as well as zebra fabrics in these dolomites, perhaps indicate a relatively calm tectonic period during dolomite development (e.g. Hollis et al., 2017).

D3 and D4 both record elevated $^{87}Sr/^{86}Sr$ ratios which accounts for their fault-controlled origin. However, their occurrence at the top of the Calcare Massiccio and overlaying Bugarone Formation (Corano Quarry site) which is < 1 m thick in Montagna dei Fiori region, and is marked as the final rift deposit (Cardello and Doglioni, 2015) discards a syn-rift origin for these dolomites. Moreover, D3 and D4 postdate the development of high amplitude ~~bed-~~bed-parallel stylolites. The formation of stylolites requires an approximate overburden of 600 to 1500 m (Lind, 1993; Machel, 1999; Mountjoy et al., 1999; Schulz et al., 2016), corresponding to a late to post-Maiolica deposition time (Early Cretaceous time onwards). The presence of D3 and D4 dolomites in ~~bed-~~bed-parallel fractures and as shear veins (D4) (Figs. 9a and b) suggests their association with contractional deformations, i.e. the most likely tectonic regime for explaining bed-perpendicular dilation. Therefore, the volumetrically minor second stage of dolomite precipitation may possibly be related to the Late- to post-Miocene compressional tectonics recorded in this region (e.g. Mazzoli et al., 2002; Artoni, 2013; Storti et al., 2018).

Dolostones containing D3 and D4 appear commonly as clast-supported breccias along fault zones pertaining to the Montagna dei Fiori Fault, then overprinted by fault-parallel stylolites (Figs. 3 and 7). Accordingly, the occurrence of these dolomites was probably synchronous with the incipient stages of fault development, predating fault buttressing (Storti et al., 2018). Homogenization temperatures recorded in D4 (up to 105°C), much higher than the maximum temperatures recorded in the host rocks (below about 80°C; Ronchi et al., 2003), suggest hydrothermal fluid circulation. The development of the Montagna dei Fiori Anticline at the toe of the Late Miocene Central Apennines thrust wedge could have favored the forelandward migration of hydrothermal fluids expelled from the more internal regions of the belt, similarly to what has been proposed for the Rocky Mountains foreland (i.e. squeegee flow model; Machel and Cavell, ~~(~~1999). Such a migration may have possibly favored the precipitation

of D4 in ~~bed~~ bed-parallel veins, generally considered as evidence for syn-compressional fluid overpressure (Sibson, 2001; Hiemstra and Goldstein, 2015). At this stage, in addition to dilation of the pre-existing ~ N-S and E-W striking rift-related extensional faults and their possible role in fluid migration, the excess of pore pressure at the base of the thrust ramp, in the fold hinge and during fold tightening could promote the localization of the fractures (Smith and Wiltschko, 1996; Ghisetti and Vezzani, 2000), with fluid migration within this zone and eventually dolomitization. These fractures could have been corridors that later on formed the insipient NW-SE Montagna dei Fiori Fault. Their localization at the back-limb cross-cutting the core, explaining best the distribution of D3 and D4 at this locality. The presence of only D5 ~~only~~ within the damage zone of the Montagna dei Fiori Fault, postdating dolostone brecciation and, in places, cementing breccia fragments~~, may~~ suggest that D5 dolomite precipitation was associated with the late stage evolution of the Montagna dei Fiori Fault, predating late stage calcite precipitation. The shift from dolomite to calcite precipitation can be ascribed to attenuation of Mg-rich fluids and/or calcite saturation. This condition was perhaps initiated during the late stages of anticline evolution due to changes in fault conductivity sealing the upward migration of Mg-rich fluids.

The presence of several generations of ~~bed~~ bed-perpendicular stylolites bounding and intersecting ~~CV2~~C2 veins (Fig. 10), supports the postulation that late stage calcite cements precipitated in close ~~closely associated~~ association with the deformation history of the Scaglia Formation in the hanging wall of the Montagna dei Fiori Fault (Fig. 3). This deformation occurred~~,~~ during buttressing against Calcare Massiccio and Corniola Formations in the footwall, and related with the positive inversion event induced by thrust-sheet stacking at depth (Storti et al., 2018). Precipitation of ~~CV3~~C3 and ~~CV4~~C4 ~~in~~ is interpreted to have occurred during uplift and cooling as revealed by their relatively low homogenization temperatures (≤ 40-50°C) of fluid inclusions trapped within these cements. Deformation twinning is either absent or weakly developed, reflecting the lack of significant tectonic deformation after calcite precipitation. These cements postdate the dolomitization events, high amplitude ~~bed~~ bed-perpendicular and parallel stylolites, and are precipitated as cements bounding the breccia fragments within the damage zone of the Montagna dei Fiori Fault. Salinities calculated from their fluid inclusions, particularly in ~~CV4~~C4, suggests precipitation from meteoric waters, which should have been favored during the late evolutionary stages of antiformal stacking beneath the Montagna dei Fiori

Anticline, and eventual late extensional slip along the Montagna dei Fiori Fault (Storti et al., 2018). The results obtained in this study are in relative agreement with the earlier work by Ronchi et al. (2003) and Murgia et al. (2004) in the Central Apennines, assigning dolomitization phases to the pre- and syn-orogenic deformations, although they did not specify the direct relation between the local structures and the different types of dolomite.

The textures of the studied dolomites vary from planar-e to non-planar, the preponderance of planar dolomite, as in D4, creates a rock with interesting poroperm characteristics (e.g. Woody et al., 1996; Wilson et al., 2007; Wenzhi et al., 2012). This case-study is certainly relevant for many potential reservoirs elsewhere in the world. Similar multistage burial dolomitization events enhancing the reservoir quality have been reported from the carbonate successions of the Jurassic in the Kopet-Dagh Basin, north eastern Iran (Adabi, 2009) and Devonian of the Rainbow sub-Basin, western Canada (Qing and Mountjoy, 1989; Lonnee, 1999).

6 Conclusions

The Lower Jurassic limestones outcropping at the core of the Montagna dei Fiori Anticline (Central Apennines, Italy) are massively affected by dolomitization, in damage zones of the pre-orogenic faults inherited from the Tethyan rifting and the ones formed during the Apenninic orogeny. Cross-cutting relationships between deformation structures, and results from optical and cold cathodoluminescence petrography, fluid inclusion microthermometry, and isotope geochemistry, support the occurrence of two major dolomitization events. The first event is interpreted as having developed during the late stages of Tethyan rifting in Jurassic and resulted in volumetrically significant dolostone geobodies. These dolostones are ~~majorly~~ largely matrix replacive, and their precipitation initiated prior to the significant burial as reflected in their cross-cutting relationship with ~~bed~~ bed-parallel stylolites, and by homogenization temperatures in fluid inclusions that are dominantly below about 40-50°C. The second dolomitization event corresponds to volumetrically less relevant replacive dolomite and dolomite cements occluding fractures. These dolomites precipitated during hydrothermal fluid circulation associated with contractional tectonics during the Apenninic orogeny, possibly at the onset of the growth of the Montagna dei Fiori Anticline (Late Miocene).

Dolomitizing fluids in both events were most likely sourced from evaporitic brines associated to the underlying Burano evaporites and their interaction with ~~siliciclastics~~ siliciclastic rocks and/or the crystalline basement.

Author contributions. M. Mozafari participated in fieldwork, performed petrographic and microthermometric analyses, provided their interpretation, and wrote the manuscript; R. Swennen participated in fieldwork, discussed the results of the diagenetic study, and critically reviewed the manuscript; F. Balsamo contributed to collect and interpret structural data, discussed structural diagenesis data interpretation, and critically reviewed the manuscript; H. El Desouky collected $^{87}Sr/^{86}Sr$ data; F. Storti conceived the research, contributed to collect and interpret structural data, discussed structural diagenesis data interpretation, and critically reviewed the manuscript; C. Taberner participated in fieldwork, discussed the results of the diagenetic study and their framing into the proposed structural evolution, and critically reviewed the manuscript.

Acknowledgments. This research was performed by collaboration between Parma and KU Leuven universities in the framework of a research project (PT12432 and GFSTE 1100942) funded by Shell Global Solutions International (Carbonate Research Team, now Geology and New Reservoir Types Team). We thank E.M. Selmo (Parma University) and M. Joachimski (University of Erlangen, Germany) for the stable carbon and oxygen analysis. G. Davis (VU Amsterdam, the Netherlands) is thanked for the strontium isotope analysis. A. Comelli and H. Nijs are kindly thanked for the careful preparation of the wafers and thin sections. L. Barchi is gratefully appreciated for his help in SEM analysis. We ~~gratefully~~ acknowledge A. Koopman for the constructive discussions during field work. We appreciate D. Smith (Energie Beheer Nederland, the Netherlands) for the careful reviewing of the manuscript. We are very grateful to reviewers J. Hendry and E. Ukar for their suggestions that allowed us to significantly improve the manuscript.

References

Adabi, M. H.: Multistage dolomitization of upper jurassic mozduran formation, Kopet-Dagh Basin, NE Iran. Carbonates and Evaporites, 24, 16-32, https://doi.org/10.1007/BF03228054, 2009.

Alvarez, W.: Evolution of the Monte Nerone Seamount in the Umbria-Marches Apennines; I, Jurassic-Tertiary stratigraphy, B. Soc. Geol. Ital., 108, 3-21, 1989.

Amieux, P.: La cathodoluminescence: méthode d'étude sédimentologique des carbonates, B. Cent. Rech. Explor.-Prod. Elf-Aquitaine, 6, 437-483, 1982.

Artoni, A.: Messinian events within the tectono-stratigraphic evolution of the Southern Laga Basin (Central Apennines, Italy), B. Soc Geol. Ital., 122, 447-466, 2003.

Artoni, A.: The Pliocene-Pleistocene stratigraphic and tectonic evolution of the central sector of the Western Periadriatic Basin of Italy, Mar. Pet. Geol., 42, 82-106, https://doi.org/10.1016/j.marpetgeo.2012.10.005, 2013.

Banner, J. L.: Radiogenic isotopes: systematics and applications to earth surface processes and chemical stratigraphy, Earth. Sci. Rev., 65, 141-194, https://doi.org/10.1016/S0012-8252(03)00086-2, 2004.

Barchi, M., Minelli, G., and Pialli G.: The CROP 03 profile: a synthesis of results of deep structures of the Northern Apennines, Mem. Soc. Geol. It., 52, 383-400, 1998.

Barker, S. L., and Cox, S. F.: Evolution of fluid chemistry and fluid-flow pathways during folding and faulting: an example from Taemas, NSW, Australia, Geol. Soc. London Spec. Publ., 359, 203-227, https://doi.org/10.1144/SP359.12, 2011.

Bassetti, M. A., Ricci Lucchi, F., Roveri, M., Taviani, M.: Messinian facies in a critical section of northern Apennines (Montepetra-Perticara, Pesaro), Giorn. Geol., 60, 261-263, 1998.

Bathurst, R. G. C. (Eds.): Carbonate sediments and their diagenesis, Dev. Sedimentol., Ser., Elsevier, 12, 658 pp., 1975.

Bathurst, R. G. C.: Deep crustal diagenesis in limestones: Revista del Instituto de Investigaciones Geologicas, Deputacion Provincial, Universidad Barcelona, 34, 89-100, 1980.

Bernoulli, D., Kälin, O., and Patacca, E.: A sunken continental margin of the Mesozoic Tethys: The Northern and Central Apennines, Symposium" Sédimentation jurassique W Européen", Spec. Publ. Ass. Sedim. Francis, 1, 179-210, 1979.

Bodnar, R. J.: Revised equation and table for determining the freezing point depression of H_2O-NaCl solutions, Geochim. Cosmochim. Acta, 57, 683-684, 10.1016/0016-7037(93)90378-A, 1993.

Boles, J. R. and Franks, S. G.: Clay diagenesis in Wilcox Sandstone of southwest Texas: Implications of smectite diagenesis and sandstone cementation, J. Sediment. Petrol., 49, 55-70, https://doi.org/10.1306/212F76BC-2B24-11D7-8648000102C1865D, 1979.

Bollati, A., Corrado, S., and Marino, M.: Inheritance of Jurassic rifted margin architecture into the Apennines Neogene mountain building: a case history from the Lucretili Mts. (Latium, Central Italy), Int. J. Earth Sci., 101, 1011-1031, https://doi.org/10.1007/s00531-011-0694-7, 2012.

Bosence, D., Procter, E., Aurell, M., Kahla, A. B., Boudagher-Fadel, M., Casaglia, F., Cirilli, S., Mehdie, M., Nieto, L., Rey, J., Scherreiks, R., Soussi, M., and Waltham, D.: A dominant tectonic signal in high-frequency, peritidal carbonate cycles? A regional analysis of Liassic platforms from western Tethys, J. Sediment. Res., 79, 389-415, https://doi.org/10.2110/jsr.2009.038, 2009.

Boschetti, T., Venturelli, G., Toscani, L., Barbieri, M., and Mucchino, C.: The Bagni di Lucca thermal waters (Tuscany, Italy): an example of $CaSO_4$ waters with high Na/Cl and low Ca/SO_4 ratios, J. Hydrol., 307, 270-293, https://doi.org/10.1016/j.jhydrol.2004.10.015, 2005.

Brandano, M., Cornacchia, I., Raffi, I., and Tomassetti, L.: The Oligocene-Miocene stratigraphic evolution of the Majella carbonate platform (Central Apennines, Italy), Sediment. Geol., 333, 1-14, https://doi.org/10.1016/j.sedgeo.2015.12.002, 2016.

Burke, W. H., Denison, R. E., Hetherington, E. A., Koepnick, R. B., Nelson, H. F., and Otto, J. B.: Variation of seawater $^{87}Sr/^{86}Sr$ throughout Phanerozoic time, Geology, 10, 516-519, https://doi.org/10.1130/0091-7613(1982)10<516:VOSSTP>2.0.CO;2, 1982.

Burkhard, M.: Calcite twins, their geometry, appearance and significance as stress-strain markers and indicators of tectonic regime: a review, J. Struct. Geol., 15, 351-368, https://doi.org/10.1016/0191-8141(93)90132-T, 1993.

Calamita, F., Cello, G., Deiana, G., and Paltrinieri, W.: Structural styles, chronology rates of deformation, and time-space relationships in the Umbria-Marche thrust system

(central Apennines, Italy), Tectonics, 13, 873-881, https://doi.org/10.1029/94TC00276, 1994.

Cardello, G. L., and Doglioni, C.: From mesozoic rifting to Apennine orogeny: the gran Sasso range (Italy), Gondwana Res., 27, 1307-1334, https://doi.org/10.1016/j.gr.2014.09.009, 2015.

Carpenter, B.: Origin and chemical evolution of brines in sedimentary basins, Oklahoma Geol. Surv., 79, 60-77, https://doi.org/10.2118/7504-MS, 1978.

Centamore, E., Chiocchini, U., and Moretti, A.. Geologia della zona tra Acerenza e Avigliano (Prov. di Potenza), Studi Geol. Camerti, 1, 97-122, http://dx.doi.org/10.15165/studgeocam-1462, 1971.

Chilovi, C., De Feyter, A. J., Minelli, G., and Barchi, M. R.. Neogene strike-slip reactivation of Jurassic normal faults in the M. Nerone-M. Catria Anticline (Umbro-Marchean Apennines, Italy), Boll. Soc. Geol. It., 121, 199-207, 2002.

Choukroune, P., Gapais, D., and Merle, O.: Shear criteria and structural symmetry, J. Struct. Geol., 9, 525-530, https://doi.org/10.1016/0191-8141(87)90137-4, 1987.

Clemenzi, L., Storti, F., Balsamo, F., Molli, G., Ellam, R., Muchez, P., and Swennen, R.: Fluid pressure cycles, variations in permeability, and weakening mechanisms along low-angle normal faults: The Tellaro detachment, Italy, Am. Assoc. Pet. Geol. Bull., 127, 1689-1710, https://doi.org/10.1130/B31203.1, 2015.

Colacicchi, R., Passeri, L., and Pialli, G.: Evidences of tidal environment deposition in the Calcare Massiccio formation (Central Apennines-Lower Lias), in: Tidal Deposits, edited by: Ginsburg, R. N., Springer, Berlin, Heidelberg, Germany, 345-353, https://doi.org/10.1007/978-3-642-88494-8, 1975.

Cooper, J. C., and Burbi, L.: The geology of the central Sibillini Mountains, Mem. Soc. Geol. It., 35, 323-347, 1986.

Crescenti, U.: Serie stratigrafiche della serie calcarea dal Lias al Miocene nella regione Marchigiano Abruzzese: parte I and II, Mem. Soc. Geol. It., 8, 155-420, 1969.

Davies, G. R., and Smith, L. B. J.: Structurally controlled hydrothermal dolomite reservoir facies: an overview, Am. Assoc. Pet. Geol. Bull., 90, 1641-1690, 2006.

Del Moro, A., Puxeddu, M., Radicati di Brozolo, F., and Villa, I. M.: Rb-Sr and K-Ar ages of minerals at temperatures of 300-400°C from deep wells in the Larderello geothermal

field (Italy), Contrib. Mineral. Petr., 81, 349-349, https://doi.org/10.1007/BF00371688, 1982.

Dewever, B., Swennen, R., and Breesch, L.: Fluid flow compartmentalization in the Sicilian fold and thrust belt: implications for the regional aqueous fluid flow and oil migration history, Tectonophysics, 591, 194-209, https://doi.org/10.1016/j.tecto.2011.08.009, 2013.

Dewey, J. F., Helman, M. L., Turco, E., Hutton, D. H. W., and Knott, S. D.: Kinematics of the western Mediterranean, in: Alpine Tectonics, edited by: Coward, M. P., Dietrich, D., Park, R. G., Geol. Soc. London Spec. Publ., 45, 265-283, https://doi.org/10.1144/GSL.SP.1989.045.01.15, 1989.

Dewit, J., Foubert, A., El Desouky, H. A., Muchez, P., Hunt, D., Vanhaecke, F., and Swennen, R.: Characteristics, genesis and parameters controlling the development of a large stratabound HTD body at Matienzo (Ramales Platform, Basque-Cantabrian Basin, northern Spain), Mar. Pet. Geol., 55, 6-25, 10.1016/j.marpetgeo.2013.12.021, 2014.

Dickson, J. A. D.: Carbonate identification and genesis as revealed by staining, J. Sediment. Petrol., 36, 491-505, https://doi.org/10.1306/74D714F6-2B21-11D7-8648000102C1865D, 1966.

Di Francesco, L., Fabbi, S., Santantonio, M., Bigi, S., and Poblet, J.: Contribution of different kinematic models and a complex Jurassic stratigraphy in the construction of a forward model for the Montagna dei Fiori fault-related fold (Central Apennines, Italy), Geol. J., 45, 489-505, https://doi.org/10.1002/gj.1191, 2010.

Eichhubl, P., and Boles, J. R.: Rates of fluid flow in fault systems; evidence for episodic rapid fluid flow in the Miocene Monterey Formation, coastal California, Am. J. Sci., 300, 571-600, doi: 10.2475/ajs.300.7.571, 2000.

Elter, P., Giglia, G., Tongiorgi, M., and Trevisan, L.: Tensional and contractional areas in the recent (Tortonian to Present) evolution of the Northern Apennines, B. Geofis. Teor. Appl., 17, 3-18, 1975.

Emery, D., and Robinson, A. (Eds.): Inorganic Geochemistry: Applications to Petroleum Geology, Blackwell Science, Oxford, United Kingdom, 101-128, 1993.

Fantoni, R., and Franciosi, R.: Tectono-sedimentary setting of the Po Plain and Adriatic foreland, Rend. Lincei , 21, 197-209, https://doi.org/10.1007/s12210-010-0102-4, 2010.

952 Ferraro, F., Agosta, F., Ukar, E., Grieco, D. S., Cavalcante, F., Belviso, C., and Prosser, G.:
953 Structural diagenesis of carbonate fault rocks exhumed from shallow crustal depths:
954 An example from the central-southern Apennines, Italy, J. Struct. Geol., 122, 58-80,
955 https://doi.org/10.1016/j.jsg.2019.02.008, 2019.
956 Flecker, R., De Villiers, S., and Ellam, R. M.: Modelling the effect of evaporation on the
957 salinity-$^{87}Sr/^{86}Sr$ relationship in modern and ancient marginal-marine systems: the
958 Mediterranean Messinian Salinity Crisis, Earth Planet. Sci. Lett., 203, 221-233,
959 10.1016/S0012-821X(02)00848-8, 2002.
960 Friedman, I.: Some investigations of the deposition of travertine from Hot Springs-I. The
961 isotopic chemistry of a travertine-depositing spring, Geochim. Cosmochim. Acta, 34,
962 1303-1315, https://doi.org/10.1016/0016-7037(70)90043-8, 1970.
963 Gale, J. F., Laubach, S. E., Marrett, R. A., Olson, J. E., Holder, J., and Reed, R. M.: Predicting
964 and characterizing fractures in dolostone reservoirs: Using the link between
965 diagenesis and fracturing, Geol. Soc. London Spec. Publ., 235, 177-192,
966 https://doi.org/10.1144/GSL.SP.2004.235.01.08, 2004.
967 Giacometti, A., and Ronchi, P.: Early Lias Carbonate Platform: Facies and Diagenesis Analogies
968 between the Calcare Massiccio (Umbro-Marchean Apennines) and the Inici Fm.
969 (Sicily Channel), Mem. Soc. Geol. It., 55, 271-278, 2000.
970 Ghisetti, F., and Vezzani, L.: Detachments and normal faulting in the Marche fold-and-thrust belt
971 (Central Apennines, Italy): inferences on fluid migration paths, J. Geodyn., 29, 345-
972 369, https://doi.org/10.1016/S0264-3707(99)00057-5, 2000.
973 Ghisetti, F., and Vezzani, L.: Interfering paths of deformation and development of arcs in the
974 fold-and-thrust belt of the central Apennines (Italy), Tectonics, 16, 523-536,
975 https://doi.org/10.1029/97TC00117, 1997.
976 Goldstein, R. H., and Reynolds, T. J.: Systematics of Fluid Inclusions in Diagenetic Minerals,
977 Soc. Sediment. Geol., Short Course, 31, 199 pp., 1994.
978 Gregg, J. M.: On the formation and occurrence of saddle dolomite-discussion, J. Sediment.
979 Petrol., 53, 1025-1033, 1983.
980 Gregg, J. M., Shelton, K. L., Johnson, A. W., Somerville, I. D., and Wright, W. R.:
981 Dolomitization of the Waulsortian limestone (lower Carboniferous) in the Irish

Midlands, Sedimentology, 48, 745-766, https://doi.org/10.1046/j.1365-3091.2001.00397.x, 2001.

Habermann, D., Neuser, R. D., and Richter, D. K.: REE-activated cathodoluminescence of calcite and dolomite: high-resolution spectrometric analysis of CL emission (HRS-CL), Sediment. Geol., 101, 1-7, https://doi.org/10.1016/0037-0738(95)00086-0, 1996.

Hendry, J. P., Gregg, J. M., Shelton, K. L., Somerville, I. D., and Crowley, S. F.: Origin, characteristics and distribution of fault-related and fracture-related dolomitization: Insights from Mississippian carbonates, Isle of Man, Sedimentology, 62, 717-752, https://doi.org/10.1111/sed.12160, 2015.

Hiemstra, E. J., and Goldstein, R. H.: Repeated injection of hydrothermal fluids into downdip carbonates: a diagenetic and stratigraphic mechanism for localization of reservoir porosity, Indian Basin Field, New Mexico, USA, Geol. Soc. London Spec. Publ., 406, 141-177, https://doi.org/10.1144/SP406.1, 2015.

Hollis, C., Bastesen, E., Boyce, A., Corlett, H., Gawthorpe, R., Hirani, J. Rotevatn, A., and Whitaker, F.: Fault-controlled dolomitization in a rift basin. Geology, 45, 219-222, https://doi.org/10.1130/G38s394.1, 2017.

Horita, J.: Oxygen and carbon isotope fractionation in the system dolomite-water-CO_2 to elevated temperatures, Geochim. Cosmochim. Acta, 129, 111-124, https://doi.org/10.1016/j.gca.2013.12.027, 2014.

Horvath, F.: Towards a mechanical model for the formation of the Pannonian basin, Tectonophysics, 226, 333-357, https://doi.org/10.1016/0040-1951(93)90126-5, 1993.

Hudson, J. D.: Stable isotopes and limestone lithification, Geol. Soc. London, 133, 637-660, https://doi.org/10.1144/gsjgs.133.6.0637, 1977.

Koopman, A.: Detachment tectonics in the central Apennines, Italy, Ph.D. thesis, Utrecht University, The Netherlands, 155 pp., 1983.

Land L. S.: The isotopic and trace element geochemistry of dolomite: the state of the art, in: Concepts and Models of dolomitization, edited by: Zenger D. H., Dunham J. B. and Ethington R. L., Soc. Econ. Paleontol. and Mineral., Spec. Pub., 28, 87-110, 1980.

Land L. S.: The application of stable isotopes to studies of the origin of dolomite and to problems of diagenesis of clastic sediments, in: Stable Isotopes in Sedimentary

1013 Geology, edited by: Arthur M. A., Soc. Econ. Paleontol. and Mineral, Short Course,
1014 10, 4-1 , 1983.
1015 Land L. S.: The origin of massive dolomite. Jour. Geol. Educ., 33, 112-125, 1985.
1016 Laubach, S. E., Eichhubl, P., Hilgers, C., and Lander, R. H.: Structural diagenesis, J. Struct.
1017 Geol., 32, 1866-1872, https://doi.org/10.1016/j.jsg.2010.10.001, 2010.
1018 Li, Z., Goldstein, R. H. and Franseen, E. K.: Meteoric calcite cementation: diagenetic response to
1019 relative fall in sea-level and effect on porosity and permeability, Las Negras area,
1020 southeastern Spain, Sediment. Geol., 348, 1-18,
1021 https://doi.org/10.1016/j.sedgeo.2016.12.002, 2017.
1022 Lind, I. L., Berger, W. H., and Kroenke, L. W.: Stylolites in chalk from leg 130, Ontong Java
1023 Plateau, in: Proceedings of the Ocean Drilling Program, scientific results, 445-451,
1024 1993.
1025 Lobato, L. M., Forman, J. M. A., Fazikawa, K., Fyfe, W. S., and Kerrich, R.: Uranium in
1026 overthrust Archean basement, Bahia, Brazil. Canadian Mineral., 21, 647-654, 1983.
1027 Lonnee, J. S.: Sedimentology, dolomitization and diagenetic fluid evolution of the Middle
1028 Devonian Sulphur Point Formation, northwestern Alberta, Ph.D. thesis, University of
1029 Windsor, Canada, 133 pp., 1999.
1030 Luczaj, J. A., and Goldstein, R. H.: Diagenesis of the Lower Permian Krider Member, southwest
1031 Kansas, USA: fluid-inclusion, U-Pb, and fission-track evidence for reflux
1032 dolomitization during latest Permian time, J. Sediment. Res., 70, 762-773,
1033 https://doi.org/10.1306/2DC40936-0E47-11D7-8643000102C1865D, 2000.
1034 Machel, H. G.: Effects of groundwater flow on mineral diagenesis, with emphasis on carbonate
1035 aquifers, Hydrol. J., 7, 94-107, https://doi.org/10.1007/s100400050, 1999.
1036 Machel, H. G., Mason, R. A., Mariano, A. N., and Mucci, A.: Causes and emission of
1037 luminescence in calcite and dolomite, in: Luminescence microscopy and
1038 spectroscopy : Qualitative and quantitative applications, edited by: Barker, C. E., and
1039 Kopp, O. C, Soc. Sediment. Geol., Short Course, 9-25, 1991.
1040 Machel, H. G., and Cavell, P. A.: Low-flux, tectonically-induced squeegee fluid flow, Bull. Can.
1041 Petrol. Geol., 47, 510-533, 1999.

1042 Major, R. P., Lloyd, R. M. and Lucia, F. J.: Oxygen isotope composition of Holocene dolomite
1043 formed in a humid hypersaline setting, Geology, 20, 586-588,
1044 https://doi.org/10.1130/0091-7613(1992)020<0586:OICOHD>2.3.CO;2, 1992.
1045 Marchegiani, L., Deiana, G., and Tondi, E.: Tettonica pre-orogenica in Appennino centrale, Stud.
1046 Geol. Camerti, 14, 211-228, http://dx.doi.org/10.15165/studgeocam-807, 1999.
1047 Marino, M., and Santantonio, M.: Understanding the geological record of carbonate platform
1048 drowning across rifted Tethyan margins: Examples from the Lower Jurassic of the
1049 Apennines and Sicily (Italy), Sediment. Geol., 225, 116-137,
1050 https://doi.org/10.1016/j.sedgeo.2010.02.002, 2010.
1051 Marshall, J. D.: Climatic and oceanographic isotopic signals from the carbonate rock record and
1052 their preservation, Geol. Mag., 129, 143-160,
1053 https://doi.org/10.1017/S0016756800008244, 1992.
1054 Mattei, M.: Analisi geologico-strutturale della Montagna dei Fiori (Ascoli Piceno, Italia
1055 Centrale), Geol. Romana, 26, 327-347, 1987.
1056 Mazzoli, S., Deiana, G., Galdenzi, S., and Cello, G.: Miocene fault-controlled sedimentation and
1057 thrust propagation in the previously faulted external zones of the Umbria-Marche
1058 Apennines, Italy, EGU Stephan Mueller Spec. Publ. Ser., 1, 195-209, 2002.
1059 Mazzullo, S. J.: Geochemical and neomorphic alteration of dolomite: a review, Carbonates
1060 Evaporites, 7, 21-37, https://doi.org/10.1007/BF03175390, 1992.
1061 McArthur, J. M., Howarth, R. J., and Shields, G. A.: Strontium isotope stratigraphy, in: The
1062 Geologic Time Scale 2012, edited by: Gradstein, F. M., Ogg, J. G., Schmitz, M., and
1063 Ogg, G., Elsevier, 127-144, https://doi.org/10.1016/C2011-1-08249-8, 2012.
1064 McCaffrey, M. A., Lazar, B., Holland, H. D.: The evaporation path of seawater and the
1065 coprecipitation of Br- and Kþ with halite, J. Sediment. Res., 57, 928-937,
1066 https://doi.org/10.1306/212F8CAB-2B24-11D7-8648000102C1865D, 1987.
1067 McCaig, A. M.: Deep fluid circulation in fault zones, Geology, 16, 867-870,
1068 https://doi.org/10.1130/0091-7613(1988)016<0867:DFCIFZ>2.3.CO;2, 1988.
1069 McCaig, A. M., Wickham, S. M., and Taylor, H. P.: Deep fluid circulation in alpine shear zones,
1070 Pyrenees, France: field and oxygen isotope studies, Contrib. Mineral. Petr., 106, 41-
1071 60, https://doi.org/10.1007/BF00306407, 1990.

1072 Montanez, I. P.: Late diagenetic dolomitization of Lower Ordovician, upper Knox carbonates: A
1073 record of the hydrodynamic evolution of the southern Appalachian Basin, Am.
1074 Assoc. Pet. Geol. Bull., 78, 1210-1239, 1994.
1075 Moore, C. H. (Eds.): Carbonate diagenesis and porosity, Dev. Sedimentol., 46, Elsevier Sci.
1076 Publ., Amsterdam, The Netherlands, 338 pp., 1989.
1077 Morettini, E., Santantonio, M., Bartolini, A., Cecca, F., Baumgartner, P. O., and Hunziker, J. C.:
1078 Carbon isotope stratigraphy and carbonate production during the Early-Middle
1079 Jurassic: examples from the Umbria-Marche-Sabina Apennines (central Italy),
1080 Paleog., Paleocl., Paleoec., 184, 251-273, https://doi.org/10.1016/S0031-
1081 0182(02)00258-4, 2002.
1082 Mountjoy, E. W., Machel, H. G., Green, D., Duggan, J., and Williams-Jones, A. E.: Devonian
1083 matrix dolomites and deep burial carbonate cements: a comparison between the
1084 Rimbey-Meadowbrook reef trend and the deep basin of west-central Alberta, B. Can.
1085 Petrol. Geol., 47, 487-509, 1999.
1086 Murgia, M. V., Ronchi, P., and Ceriani, A.: Dolomitization processes and their relationships with
1087 the evolution of an orogenic belt (Central Apennines and peri-adriatic foreland,
1088 Italy), AAPG Hedberg series, 1, 277-294, https://doi.org/10.1306/1025695H13121,
1089 2004.
1090 Nelson, R. A: Significance of fracture sets associated with stylolite zones, Am. Assoc. Pet. Geol.
1091 Bull., 65, 2417-2425, 1981.
1092 Parotto, M., and Praturlon, A.: Geological summary of the Central Apennines, Quad. Ric. Sci.,
1093 90, 257-311, 1975.
1094 Patacca, E., Sartori, R., and Scandone, P.: Tyrrhenian basin and Apenninic arcs: Kinematic
1095 relations since late Tortonian times, Mem. Soc. Geol. It., 45, 425-451,
1096 http://hdl.handle.net/11568/11610, 1992.
1097 Pialli, G.: Facies di piana cotidale nel Calcare Massiccio dell'Appennino umbro marchigiano,
1098 Boll. Soc. Geol. It., 90, 481-507, 1971.
1099 Pierantoni, P., Deiana, G., and Galdenzi, S.: Stratigraphic and structural features of the Sibillini
1100 Mountains (Umbria-Marche Apennines, Italy), Ital. J. Geosci., 132, 497-520,
1101 https://doi.org/10.3301/IJG.2013.08, 2013.

1102 Purser, B., Tucker, M. and Zenger, D.: Problems, progress and future research concerning
1103 dolomites and dolomitization, in: Dolomites: a Volume in Honour of Dolomieu,
1104 edited by: Purser, B., Tucker, M. and Zenger, D., IAS Spec. Publ., 21, 3-20, 1994.
1105 Qing, H., and Mountjoy, E. W.: Multistage dolomitization in Rainbow buildups, Middle
1106 Devonian Keg River Formation, Alberta, Canada. J. of Sediment. Res., 59, 114-126,
1107 https://doi.org/10.1306/212F8F30-2B24-11D7-8648000102C1865D, 1989.
1108 Radke, B. M., and Mathis, R. L.: On the formation and occurrence of saddle dolomite, J.
1109 Sediment. Res., 50, 1149-1168, https://doi.org/10.1306/212F7B9E-2B24-11D7-
1110 8648000102C1865D, 1980.
1111 Ronchi, P., Casaglia, F., and Ceriani, A.: The multiphase dolomitization of the Liassic Calcare
1112 Massiccio and Corniola successions (Montagna dei Fiori, Northern Apennines, Italy),
1113 Boll. Soc. Geol. It., 122, 157-172, 2003.
1114 Rosenbaum, J., and Sheppard, S. M.: An isotopic study of siderites, dolomites, and ankerites at
1115 high temperatures, Geochim. Cosmochim. Acta, 50, 1147-1150,
1116 https://doi.org/10.1016/0016-7037(86)90396-0, 1986.
1117 Roveri, M., Bassetti, M. A., and Lucchi, F. R.: The Mediterranean Messinian salinity crisis: an
1118 Apennine foredeep perspective, Sediment. Geol., 140, 201-214,
1119 https://doi.org/10.1016/S0037-0738(00)00183-4, 2001.
1120 Saelen, G., Doyle, P., and Talbot, M. R.: Stable-isotope analyses of belemnite rostra from the
1121 Whitby Mudstone Fm., England: Surface water conditions during deposition of a
1122 marine black shale, Palaios, 11, 97-117, https://doi.org/10.2307/3515065, 1996.
1123 Santantonio, M, and Carminati, E.: Jurassic rifting evolution of the Apennines and Southern Alps
1124 (Italy): Parallels and differences, Geol. Soc. Am. B., 123, 464-484,
1125 https://doi.org/10.1130/B30104.1, 2011.
1126 Santantonio, M. and Muraro, C.: The Sabina Plateau, Palaeoescrapment, and Basin-Central
1127 Apennines, 6th international symposium on the Jurassic system, General Field Trip
1128 Guidebook, Palermo, Italy, 271-315, 2002.
1129 Santantonio, M., Fabbi, S., and Bigi, S.: Discussion on «Geological map of the partially
1130 dolomitized Jurassic succession exposed in the central sector of the Montagna dei
1131 Fiori Anticline, Central Apennines, Italy», Ital. J. Geosci., 136, 312-316,
1132 https://doi.org/10.3301/IJG.2017.04, 2017.

1133 Schulz, H. M., Wirth, R., and Schreiber, A.: Organic-inorganic rock-fluid interactions in
1134 stylolitic micro-environments of carbonate rocks: a FIB-TEM study combined with a
1135 hydrogeochemical modelling approach, Geofluids, 16, 909-924,
1136 https://doi.org/10.1111/gfl.12195, 2016.
1137 Scisciani V., Tavarnelli, E., and Calamita, F.: The interaction of extensional and contractional
1138 deformations in the outer zones of the Central Apennines, Italy, J. Struct. Geol., 24,
1139 1647-1658, https://doi.org/10.1016/S0191-8141(01)00164-X, 2002.
1140 Shackleton, N. J., and Kennett, J. P.: Paleotemperature History of the Cenozoic and the Initiation
1141 of Antartic Glaciation Oxygen and Carbon Isotope Analyses in DSDP Sites 277, 279,
1142 and 281, Initial reports of Deep Sea Drilling Project, 29, 743-755, 1975.
1143 Sharp, I., Gillespie, P., Morsalnezhad, D., Taberner, C., Karpuz, R., Vergés, J., Horbury, A.,
1144 Pickard, N., J. Garland, J., and Hunt, D.: Stratigraphic architecture and fracture-
1145 controlled dolomitization of the Cretaceous Khami and Bangestan groups: an outcrop
1146 case study, Zagros Mountains, Iran, Geol. Soc. London Spec. Publ., 329, 343-396,
1147 https://doi.org/10.1144/SP329.14, 2010.
1148 Shepherd, T., Rankin, A. H., and Alderton, D. H. M. (Eds.): A Practical Guide to Fluid Inclusion
1149 Studies, Glasgow: Blackie, 239 pp., 1985.
1150 Sibley, D. F., and Gregg, J. M.: Classification of dolomite rock textures, J. Sediment. Petrol., 57,
1151 967-975, https://doi.org/10.1306/212F8CBA-2B24-11D7-8648000102C1865D,
1152 1987.
1153 Sibson, R. H.: Fluid flow accompanying faulting: field evidence and models, Earthquake
1154 prediction: an international review, AGU, 4, 593-603,
1155 https://doi.org/10.1029/ME004p0593, 1981.
1156 Slobodník, M., Muchez, P., Kral, J., and Keppens, E.: Variscan veins: record of fluid circulation
1157 and Variscan tectonothermal events in Upper Palaeozoic limestones of the Moravian
1158 Karst, Czech Republic, Geol. Mag., 143, 491-508,
1159 https://doi.org/10.1017/S0016756806001981, 2006.
1160 Smith, R. E., Wiltschko, D. V.: Generation and maintenance of abnormal fluid pressures beneath
1161 a ramping thrust sheet: isotropic permeability experiments, J. Struct. Geol., 18, 951-
1162 970, https://doi.org/10.1016/0191-8141(96)00023-5, 1996.

1163 Steiger, R., and Jäger, E.: Subcommission on geochronology: convention on the use of decay
1164 constants in geo and cosmochronology, Earth Planet. Sci. Lett., 36, 359-362,
1165 https://doi.org/10.1016/0012-821X(77)90060-7, 1977.
1166 Storti, F., Balsamo, F., and Koopman, A.: Geological map of the partially dolomitized Jurassic
1167 succession exposed in the core of the Montagna dei Fiori Anticline, Central
1168 Apennines, Italy, Ital. J. Geosci., 136, 125-135, https://doi.org/10.3301/IJG.2016.05,
1169 2017a.
1170 Storti F., Balsamo, F., and Koopman, A.: Reply to: discussion on «Geological map of the
1171 partially dolomitized Jurassic succession exposed in the central sector of the
1172 Montagna dei Fiori Anticline, Central Apennines, Italy» by Santantonio, M., Fabbi,
1173 S. and Bigi, S., Ital. J. Geosci., 136, 317-319, https://doi.org/10.3301/IJG.2017.04,
1174 2017b.
1175 Storti, F., Balsamo F., Mozafari M., Koopman A., Swennen R. and Taberner C.: Syn-
1176 contractional overprinting between extension and shortening along the Montagna dei
1177 Fiori Fault during Plio-Pleistocene antiformal stacking at the Central Apennines
1178 thrust wedge toe, Tectonics, https://doi.org/10.1029/2018TC005072, 2018.
1179 Stueber, A. M., Pushkar, P., and Baldwin, A. D., JR.: Survey of $^{87}Sr/^{86}Sr$ ratios and total
1180 strontium concentrations in Ohio stream and ground waters, Ohio J. Sci., 72, 98-104,
1181 1972.
1182 Sommer, S. E.: Cathodoluminescence of carbonates, 1. Characterization of cathodoluminescence
1183 from carbonate solid solutions, Chemical Geology, 9, 257-273,
1184 https://doi.org/10.1016/0009-2541(72)90064-2, 1972.
1185 Swennen, R., Dewit, J., Fierens, E., Muchez, Ph., Shah, M., Nader, F. H., Hunt, D.: Multiple
1186 dolomitisation events along the Ranero fault (Pozalagua Quarry, BasqueeCantabrian
1187 Basin): episodic earthquake activity, Sedimentology, 59, 1345-1374,
1188 https://doi.org/10.1111/j.1365-3091.2011.01309.x, 2012.
1189 Tavani, S., Storti, F., Salvini, F., and Toscano, C.: Stratigraphic versus structural control on the
1190 deformation pattern associated with the evolution of the Mt. Catria anticline, Italy, J.
1191 Struct. Geol., 30, 664-681, https://doi.org/10.1016/j.jsg.2008.01.011, 2008.

1192 Taylor, H. P.: Oxygen and hydrogen isotope relationships in hydrothermal mineral deposits, In:
1193 Geochemistry of hydrothermal ore deposits, edited by: Barnes, H. L., Wiley and
1194 Sons, New york, 229-302, 1997.
1195 Thirlwall, M. F.: Long-term reproducibility of multicollector Sr and Nd isotope ratio analysis,
1196 Chemical Geology, 94, 85-104, https://doi.org/10.1016/S0009-2541(10)80021-X,
1197 1991.
1198 Tongiorgi, M., Rau, A., and Martini, I. P.: Sedimentology of early-alpine, fluvio-marine, clastic
1199 deposits (Verrucano, Triassic) in the Monti Pisani (Italy), Sediment. Geol., 17, 311-
1200 332, https://doi.org/10.1016/0037-0738(77)90051-3, 1977.
1201 Ukar, E., and Laubach, S. E.: Syn-and postkinematic cement textures in fractured carbonate
1202 rocks: Insights from advanced cathodoluminescence imaging, Tectonophysics, 690,
1203 190-205, https://doi.org/10.1016/j.tecto.2016.05.001, 2016.
1204 Vai, G. B., and Ricci Lucchi, F.: Algal crusts, autochthonous and clastic gypsum in a
1205 cannibalistic evaporite basin: a case history from the Messinian of northern
1206 Apennines. Sedimentology, 24, 221-244, https://doi.org/10.1111/j.1365-
1207 3091.1977.tb00255.x, 1977.
1208 Vandeginste, V., Swennen, R., Gleeson, S. A., Ellam, R. M., Osadetz, K., and Roure, F.: Zebra
1209 dolomitization as a result of focused fluid flow in the Rocky Mountains Fold and
1210 Thrust Belt, Canada. Sedimentology, 52, 1067-1095, https://doi.org/10.1111/j.1365-
1211 3091.2005.00724.x, 2005.
1212 Vandeginste, V., Swennen, R., Gleeson, S. A., Ellam, R. M., Osadetz, K., and Roure, F.:
1213 Geochemical constraints on the origin of the Kicking Horse and Monarch Mississippi
1214 Valley-type lead-zinc ore deposits, southeast British Columbia, Canada, Mineralium
1215 Deposita, 42, 913-935, https://doi.org/10.1007/s00126-007-0142-6, 2007.
1216 Veizer, J., Ala, D., Azmy, K., Bruckshen, P., Buhl, D., Bruhn, F., Carden, G. A. F., Diener, A.,
1217 Ebneth, S., Godderis, Y., Jasper, T., Korte, C., Pawellek, F., Podlaha, O. G., and
1218 Strauss, H.: $^{87}Sr/^{86}Sr$, $\delta^{13}C$ and evolution of Phanerozoic seawater, Chemical
1219 Geology, 161, 59-88, https://doi.org/10.1016/S0009-2541(99)00081-9, 1999.
1220 Walker, G., Abumere, O. E., and Kamaluddin, B.: Luminescence spectroscopy of Mn2 rock-
1221 forming carbonates, Mineral. Mag., 53, 201-11, 10.1180/minmag.1989.053.370.07,
1222 1989.

Wenzhi, Z., Anjiang, S., Suyun, H., Baomin, Z., Wenqing, P., Jingao, Z. and Zecheng, W.: Geological conditions and distributional features of large-scale carbonate reservoirs onshore China. Petrol. Explor. Develop., 39, 1-14, https://doi.org/10.1016/S1876-3804(12)60010-X, 2012.

Wilson, A., and Ruppel, C.: Salt tectonics and shallow subsea floor fluid convection: models of coupled fluid-heat-salt transport, Geofluids, 7, 377-386, https://doi.org/10.1111/j.1468-8123.2007.00191.x, 2007.

Wilson, M. E. J., Evans, M. J., Oxtoby, N. H., Nas, D. S., Donnelly, T. and Thirlwall, M.: Reservoir quality, textural evolution, and origin of fault-associated dolomites. AAPB Bull., 91, 1247-1272, 2007.

Woodcock, N. H., and Mort, K.: Classification of fault breccias and related fault rocks, Geol. Mag., 145, 435-440, https://doi.org/10.1017/S0016756808004883, 2008.

Woody, R. E., Gregg, J. M. and Koederitz, L. F.: Effect of texture on petrophysical properties of dolomite: Evidence from the Cambrian-Ordovician of Southeastern Missouri. AAPG Bull., 80, 119-131, 1996.

Zempolich, W. G., and Hardie, L. A.: Geometry of dolomite bodies within deep-water resedimented oolite of the Middle Jurassic Vajont Limestone, Venetian Alps, Italy: Analogs for hydrocarbon reservoirs created through fault-related burial dolomitization, in: Reservoir quality prediction in sandstones and carbonates, edited by: Kupecz, A., Gluyas, J., and Bloch, S., AAPG Mem., 69, 127-162, 1997.

Table captions

Table. 1. Stable carbon and oxygen isotopes, $^{87}Sr/^{86}Sr$ ratios, and fluid inclusion microthermometry data (not pressure corrected) of host rocks and diagenetic phases in the Montagna dei Fiori Anticline. Stable carbon and oxygen isotopes values are expressed in ‰ V-PDB and salinity values in eq. wt. % NaCl.

Figure captions

Fig. 1. ~~A~~a) Simplified regional map (modified after Ghisetti and Vezzani, 1997) showing the tectonic outlines of the Central Apennines and the study area (rectangle). ~~B~~b) Schematic geological map of the Montagna dei Fiori Anticline showing the distribution of dolostones (modified after Storti et al., 2017a). ~~C~~c) Lithostratigraphical column of the successions exposed in Montagna dei Fiori (modified after Mattei, 1987; Di Francesco et al, 2010; Storti et al., 2018). Letter *B* stands for the Bugarone Formation. Lithologies are mentioned in the text. Note that the thickness of the not-outcropping formations (Triassic evaporites and the crystalline basement) is not to scale. ~~D~~d) Regional ~~Geological~~ geological transect across present day Central Apennines and the Adriatic Sea (modified after Fantoni and Franciosi, 2010) with vertical exaggeration of 2:1. The dashed rectangle indicates the Montagna dei Fiori Anticline region.

Fig. 2. ~~A~~a, ~~B~~b) Geological map of the central sector of the Montagna dei Fiori Anticline, and cross-section oriented parallel (a-b) to the hinge line representing the tectono-stratigraphic architecture of the faulted anticline (modified after Storti et al., 2017a). The stereonets (Schmidt equal area projection lower hemisphere) provide the attitude of the extensional faults. The locations of the corresponding field sites are indicated by ~~numbers~~letters. c) At this location, well exposed N-S striking extensional fault zones offset the dolomitized Corniola Formation. The fault zone is characterized by near-horizontal stylolites localized in the footwall damage zone (4 fault data). d, e and f) These locations consist of mostly ~ E-W striking extensional fault zones. Particularly the boundary fault zones delimiting Calcare Massiccio Formation in the main horst block is evident (site d: 20 fault data; site e: 24 fault data; site f: 9 fault data). g and h) At these locations, dip-slip slickenlines support major extensional movements related to the Montagna dei Fiori Fault. Contractional deformation structures are preserved in the bed-perpendicular

stylolites, shear surfaces and tension gashes arranged as S-C arrays (site g: 21 fault data; site h: 14 fault data). Equal area projection, lower hemisphere.

Fig. 3. ~~A~~a) Field photograph showing the deformed Scaglia Formation in the hanging wall (HW) and brecciated, dolomitized Calcare Massiccio Formation in the footwall (FW) of the Montagna dei Fiori Fault. The red arrow indicates the sense of fault movement. ~~B~~b) A hand specimen from the deformed Scaglia formation showing ~~the intensity of the~~abundant pressure ~~solutions~~ solution seems (TS), indicated by arrows, ~~and their abutting relationship with~~cross-cutting calcite veins (~~CV2~~C2). ~~C~~c) A transmitted light photomicrograph of the dolomitized, brecciated Calcare Massiccio Formation. Note all the breccia fragments are composed of dolomite (D4 here).

Fig. 4. Field photographs (Corano Quarry) showing the field relations between dolostones (only D3 here), host limestones and the Montagna dei Fiori Fault: ~~A~~a) Panoramic view showing the spatial relationship between limestones and dolostones (orange) in the damage zone of the Montagna dei Fiori Fault (F). Note that the limestones and including dolostones of the Calcare Massiccio and Bugarone Formations on the footwall (FW) and marly limestones of the Scaglia Formation on the hangingwall (HW) are intensely deformed. ~~B~~b) Plan view of the dolomitized Calcare Massiccio limestone in the footwall damage zone: intersected by calcite veins (~~CV1~~C1~~),~~) which are partially dolomitized, and affected by ~~bed~~ bed-perpendicular stylolites (arrows). ~~C~~c) Distinct transition (dashed line) between dolomitized and undolomitized Calcare Massiccio limestone in the footwall damage zone.

Fig. 5. Field photograph (~~A~~a) and a simplified sketch (~~B~~b) in field site d showing ~~of~~ a dolomitic pocket (grey color) ~~within the folded Calcare Massiccio (grey color)~~ and ~~their~~ its relation with ~~bed~~ bed-parallel stylolites within the Calcare Massiccio Formation (hammer is 40 cm long). Note C1 is the only calcite cement here.

Fig. 6. Undolomitized and dolomitized Calcare Massiccio Formation in field site d: ~~A~~a) Transmitted light image showing a micritic peloid rimmed by ~~the~~ fibrous cements (FC) which are ~~followed~~ overgrown by ~~the~~ mosaic cements (MC). ~~B~~b) Transmitted light image showing mosaic cements (MC) in a peloidal limestone over-printed by high amplitude ~~bed~~ bed-parallel

stylolites (dotted white line). Note the core of some of the peloids is partially cemented as well. ~~C~~c, ~~D~~d) Respectively, transmitted light and corresponding cathodoluminescence image of FC and MC cements. ~~E~~e) Transmitted light photomicrograph showing D1 crystals (arrows) ~~rimming~~ lining a fracture which is cemented by ~~CV1~~C1. The fracture is in turn affected by a ~~bed-~~bed-parallel stylolite. ~~F~~f) Cathodoluminescence image showing D1 scattered in the host rock and riming the fracture. ~~G~~g, ~~H~~h) Respectively, transmitted light and corresponding cathodoluminescence image showing part of a ~~bed-~~bed-parallel stylolite (dotted white line) overprinting D1 and D2 crystals.

Fig. 7. ~~A~~a, ~~B~~b) Photomicrographs of respectively, transmitted light and corresponding cathodoluminescence image showing the zoned rhombs of D2 with the remnants of D1 preserved in their cloudy core sampled from dolomitized Calcare Massiccio Formation in field site d. The pore space is occluded by D4. ~~C~~c, ~~D~~d) D3 cementing angular breccia fragments of the Bugarone Formation in the damage zone of the Montagna dei Fiori Fault in the Corano Quarry site. Note the breccia is overprinted by a ~~fault-~~fault-parallel ~~bed-~~bed-perpendicular stylolite. ~~E~~e, ~~F~~f) Photomicrographs of respectively, transmitted light and corresponding cathodoluminescence image showing the euhedral to subhedral crystals of D3 entirely replacing the matrix and also present as cement developing a bright subzone and rim sampled from dolomitized Corniola Formation in Osso-caprino road. ~~G~~g, ~~H~~h) D3 with a saddle crystal outline (SD) postdating calcite cements (MC) and a zoned D2 crystal. The saddle morphology is outlined by a dotted white line.

Fig. 8. Photomicrographs of respectively, transmitted light and corresponding cathodoluminescence image of dolomite types: ~~A~~a, ~~B~~b) The cross-cutting relationship between D3 and D4 sampled from dolomitized Corniola Formation in Osso-caprino road. Note the presence of D3 within the core of dolomite crystals overgrown by D4. ~~C~~c, ~~D~~d) Successions of dolomite types sampled from dolomitized Calcare Massiccio Formation in field site f. Note the green CL color of D4 crystals. Typically, luminescent dolomites are known to show yellow, orange to red colors (Machel et al., 1991). Green luminescence in carbonates including dolomite have been attributed by a number of researchers to the incorporation of three valent rare earth elements (REE) such as Dy^{3+} and U^{3+} as luminescence activators within their crystal lattice (Luczaj and Goldstein, 2000). Another possibility is the emplacement of Mn^{2+}, with yellow

luminescence, in Ca^{2+} sites with blue luminescence in the dolomite crystal lattice instead of preferential incorporation in the Mg^{2+} site (Sommer, 1972b; Amieux, 1982; Walker et al., 1989; Habermann et al., 1999). Accordingly, non-stoichiometric, Ca-rich and poorly ordered dolomites may favor Mn^{+2} incorporation into their Ca^{2+} site. ~~E~~e, ~~F~~f) Vuggy porosity rimmed by D4 (green CL). Note the porosity is filled with fine dolomite rhombs including traces of D2 in their core and D4 overgrowths.

Fig. 9. Photomicrographs showing respectively, transmitted light and corresponding cathodoluminescence image of D4 and D5 in relation to stylolites and fracturing: ~~A~~a, ~~B~~b) D4, exploiting a ~~bed~~ bed-parallel stylolite that crossed-cuts D1 and D2 sampled from dolomitized Calcare Massiccio Formation in field site d. ~~C~~c, ~~D~~d) A sub-horizontal fracture cemented by D4 sampled from dolomitized Corniola Formation in field site f. ~~E~~e, ~~F~~f) D5 microveins (arrows) intersecting all the predating dolomite types in the footwall brecciated zone of the Montagna dei Fiori Fault~~.~~, sampled from dolomitized Calcare Massiccio Formation in Castel Manfrino site.

Fig. 10. Field photographs showing the major calcite vein settings observed in Montagna dei Fiori: ~~A~~a) Cross-sectional view of bed normal Calcite vein 1 (~~CV1~~C1) abutting ~~bed~~ bed-parallel stylolites in folded beds of the Calcare Massiccio Formation. ~~B~~b) Plan view of the Calcite vein 2 (~~CV2~~C2) intensely affecting the deformed Scaglia (Rossa) Formation. ~~C~~c, ~~D~~d) Cross-sectional view of the Scaglia Formation, intensely affected by pressure solution seams of tectonic origin crossed-over by populations of bed-perpendicular Calcite veins (~~CV3~~C3) in en echelon extensional arrays.

Fig. 11. ~~A~~a) Cathodoluminescence and transmitted light (in set) image showing blocky to elongated crystals of ~~CV1~~C1 with zoned CL pattern in the Corano Quarry site. ~~B~~b) Transmitted light image showing intensely twinned ~~CV1~~C1 crystals overprinted by euhedral to subhedral crystals of D3 in the Corano Quarry site. Photomicrographs of respectively, transmitted light and corresponding cathodoluminescence image: ~~C~~c, ~~D~~d) ~~CV2~~C2 in the Scaglia Formation abutted by a ~~bed~~ bed-perpendicular stylolite (indicated by white arrows and dashed line) in the Corano Quarry site. The crystals display blocky to fibrous morphologies, deformation twinning, and a similar orange luminescence pattern ~~comparable with~~similar to the adjacent host rock. ~~E~~e, ~~F~~f)

~~CV3~~C3 cementing the breccia fragments in the damage zone of the Montagna dei Fiori Fault. The crystals are blocky and show faint deformation twinning. They are brown-orange with distinct darker luminescence sector zones. ~~G~~g, ~~H~~h) ~~CV4~~C4 present as a cement within a polygonal pore space rimmed by dolomite~~.~~, sampled from dolomitized Calcare Massiccio Formation in field site f. Note the blocky crystals, absence of deformation twinning and distinct concentric luminescence zonation pattern. ~~CV4~~C4 is corroded and followed by a late telogenetic calcite.

Fig. 12. ~~A , B)~~ Overview of the $\delta^{13}C$ and $\delta^{18}O$ values of dolomites (~~A~~a) host rocks from Montagna dei Fiori as well as calcite veins (~~B~~b). The stable isotope value of Lower Jurassic marine limestones based on Veizer et al. (1999) is indicated by a dashed rectangle in subset B. The $\delta^{18}O$ values of the marine dolomites are considered to be 3-4‰ V-PDB higher than those of marine limestones (Land, 1980; Major et al., 1992; Horita, 2014). ~~C~~c) Cross-plot of $^{87}Sr/^{86}Sr$ ratios and corresponding $\delta^{18}O$ values of host rocks, dolomites and calcite veins compared with Lower Jurassic marine carbonates $^{87}Sr/^{86}Sr$ (dashed rectangle) framework reported by McArthur et al. (2012).

Fig. 13. Overview of microthermometry analysis of primary inclusions in Montagna dei Fiori: ~~A~~a) Frequency distribution of the Tm_{ice} (°C) in dolomite ~~phases~~types. ~~B~~b) Frequency distribution of the Th (°C) in dolomite ~~phases~~types. ~~C~~c) Salinity (eq. wt. % NaCl) versus Th (°C) of dolomite and calcite phases. ~~D~~d) Isotopic fractionation diagram from Land (1983) used to determine the isotopic composition (‰ V-SMOW) of parental fluids in equilibrium with dolomites in Montagna dei Fiori.

Fig. 14. ~~A)~~ Generalized paragenesis of diagenetic phases in relation to deformational stages and burial history of the Calcare Massiccio Formation in the Montagna dei Fiori Anticline. The deformational stages are from Storti et al. (2018), and the burial curve is based on Ronchi et al. (2003). The burial curve was made based on paleo-depth, paleo-temperatures, sedimentation rate and paleo-heat flow.

Fig. 15. Sketch showing the successive fault-related diagenetic phases, of most importantly dolomitization, recorded in the carbonate succession exposed at the core of the Montagna dei Fiori Anticline (not scaled). Different diagenetic phases are indicated with different colors. ~~A~~a) The first dolomitization event is pre-orogenic (syn-rift), triggered from the fluids channelized along Jurassic ~ E-W and ~ N-S striking extensional faults. This event occurred during burial compaction and development of ~~bed-~~bed-parallel stylolites (BS). It is represented by scattered dolomite rhombs (D1) followed by calcite cementation (~~CV1~~C1). The dolomitization continued with precipitation of larger crystals of D2. ~~B~~b) Second dolomitization event: syn-orogenic (early folding/ faulting) dolomitization from fluids that migrated from more internal regions of the thrust belt and were channelized along the basal detachment level into the fold core. This dolomitization event presents matrix replacive and cements displaying infrequent saddle outlines (SD) in pore spaces, within ~~bed-~~bed-parallel veins and shear fractures. These dolostones postdate compaction but are affected by ~~bed-~~bed-perpendicular stylolites (TS) generated by horizontal to sub-horizontal ~~layer-~~layer-parallel shortening related to the growth of the Montagna dei Fiori Anticline. ~~C~~c) Extensional collapse of the anticline and development of the Montagna dei Fiori Fault, followed by buttressing of the Scaglia against Calcare Massiccio and Corniola Formations during positive inversion induced by continuing underthrusting at depth. Precipitation of D5 in micro-veins and cements in breccia zones, followed by late stage calcite cementation in the Montagna dei Fiori Fault damage zone (~~CV2~~C2, ~~CV3~~C3 and ~~CV4~~C4).

	Stable isotopes		Sr isotopes	Fluid inclusion microthermometry		
	$\delta^{13}C$	$\delta^{18}O$	$^{87}Sr/^{86}Sr$	Th (°C)	Salinity	n
Calcare Massiccio Fm.	+2.4 to +3.1	-1.6 to 0.0	0.70766	-	-	
Corniola Fm.	+2.0 to +2.5	-3.1 to -1.4	0.70725	-	-	
Scaglia Fm.	+1.0 to +3.1	-2.2 to -1.0	0.70784-0.70791	-	-	
D1	+2.5	-1.9	0.70789	≤ 40-50	3.5 to 11.3	27
CV1	+1.6 to +2.1	-4.7 to -2.7	0.70773	-	-	-
D2	-	-	-	≤ 40-50 to 71	7.9 to 20.5	37
D3	+2.0 to +2.6	-2.8 to -1.9	0.70859-0.70964	70 to 73	9.2 to 16.9	9
D4	+2.4 to +2.5	-3.0 to -2.5	0.70790	79 to 105	12.8 to 18.6	7
CV2	+1.2 to +3.1	-1.7 to -1.6	0.70779 - 0.70787	-	-	
CV3	+0.5 to +2.4	-2.2 to 0.0	-	≤ 40-50	4.5 to 9.7	9
CV4	+3.8 to +4.9	-9.4 to -9.1	-	≤ 40-50	0.17 to 3.0	19

Table. 1

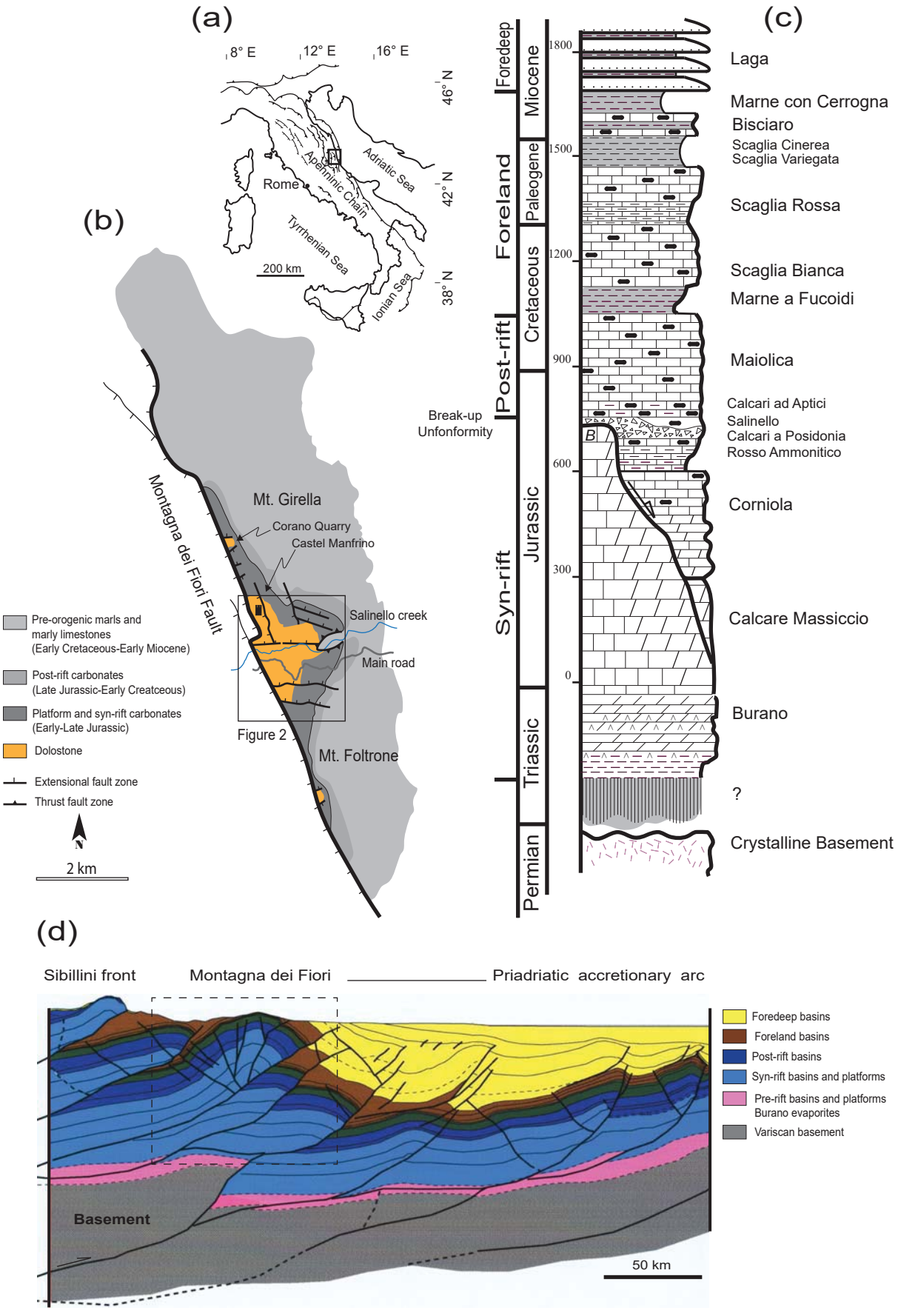
(a)
8° E
12° E
16° E
46° N
42° N
38° N
Rome
Apennine Chain
Adriatic Sea
Tyrrhenian Sea
Ionian Sea
200 km
(b)
Montagna dei Fiori Fault
Mt. Girella
Corano Quarry
Castel Manfrino
Salinello creek
Main road
Figure 2
Mt. Foltrone
Pre-orogenic marls and marly limestones (Early Cretaceous-Early Miocene)
Post-rift carbonates (Late Jurassic-Early Creatceous)
Platform and syn-rift carbonates (Early-Late Jurassic)
Dolostone
Extensional fault zone
Thrust fault zone
N
2 km
(c)
Foredeep
Foreland
Post-rift
Syn-rift
Miocene
Paleogene
Cretaceous
Jurassic
Triassic
Permian
Break-up Unfonformity
1800
1500
1200
900
600
300
0
B
Laga
Marne con Cerrogna
Bisciaro
Scaglia Cinerea
Scaglia Variegata
Scaglia Rossa
Scaglia Bianca
Marne a Fucoidi
Maiolica
Calcari ad Aptici
Salinello
Calcari a Posidonia
Rosso Ammonitico
Corniola
Calcare Massiccio
Burano
?
Crystalline Basement
(d)
Sibillini front
Montagna dei Fiori
Priadriatic accretionary arc
Basement
50 km
Foredeep basins
Foreland basins
Post-rift basins
Syn-rift basins and platforms
Pre-rift basins and platforms
Burano evaporites
Variscan basement

Fig. 1

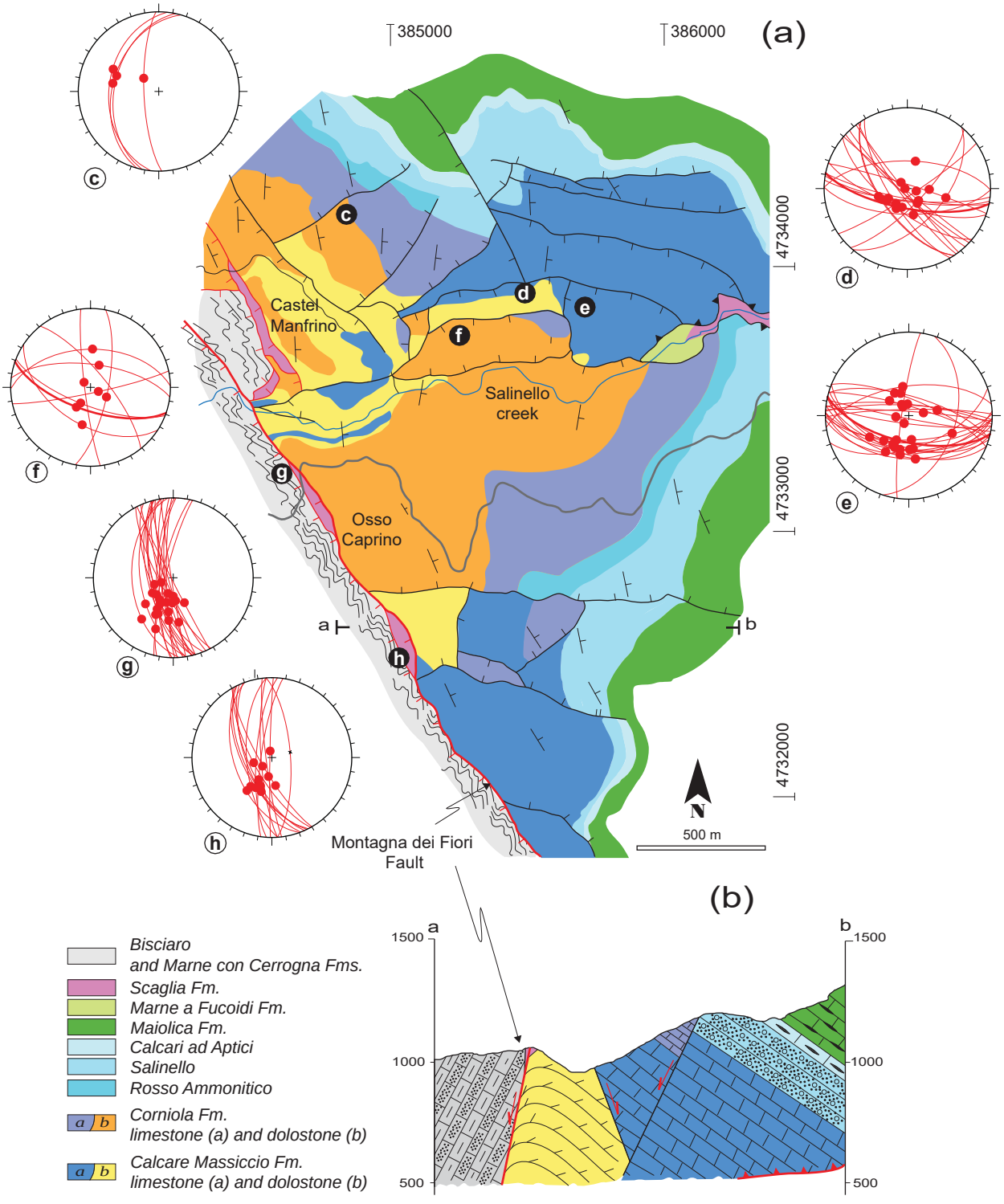
385000
386000
(a)
4734000
4733000
4732000
Castel
Manfrino
Salinello
creek
Osso
Caprino
Montagna dei Fiori
Fault
a
b
N
500 m
(b)
1500
1000
500
Bisciaro
and Marne con Cerrogna Fms.
Scaglia Fm.
Marne a Fucoidi Fm.
Maiolica Fm.
Calcari ad Aptici
Salinello
Rosso Ammonitico
Corniola Fm.
limestone (a) and dolostone (b)
Calcare Massiccio Fm.
limestone (a) and dolostone (b)

Fig. 2

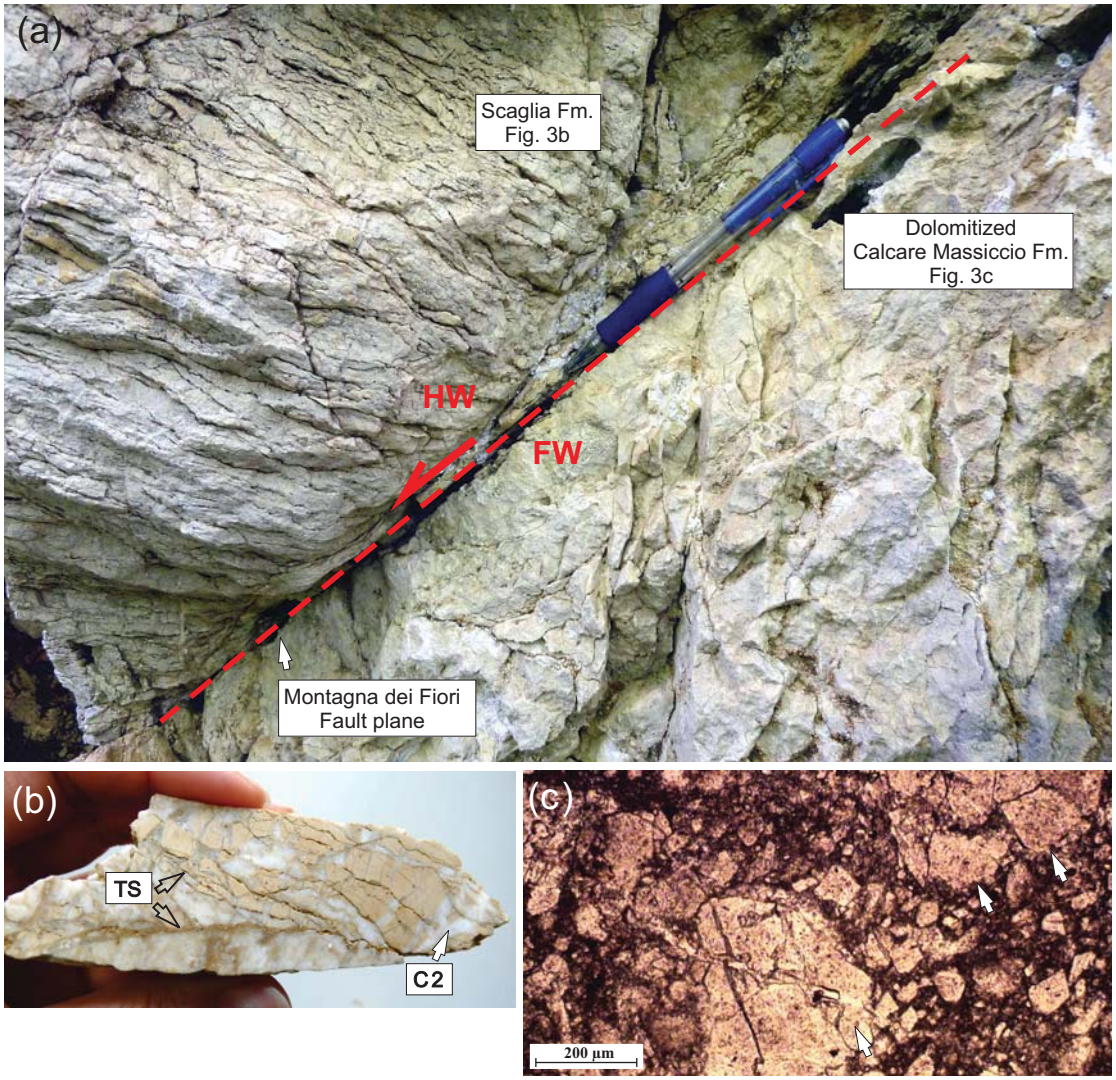
(a)
Scaglia Fm.
Fig. 3b
Dolomitized
Calcare Massiccio Fm.
Fig. 3c
HW
FW
Montagna dei Fiori
Fault plane
(b)
TS
C2
(c)
200 µm

Fig. 3

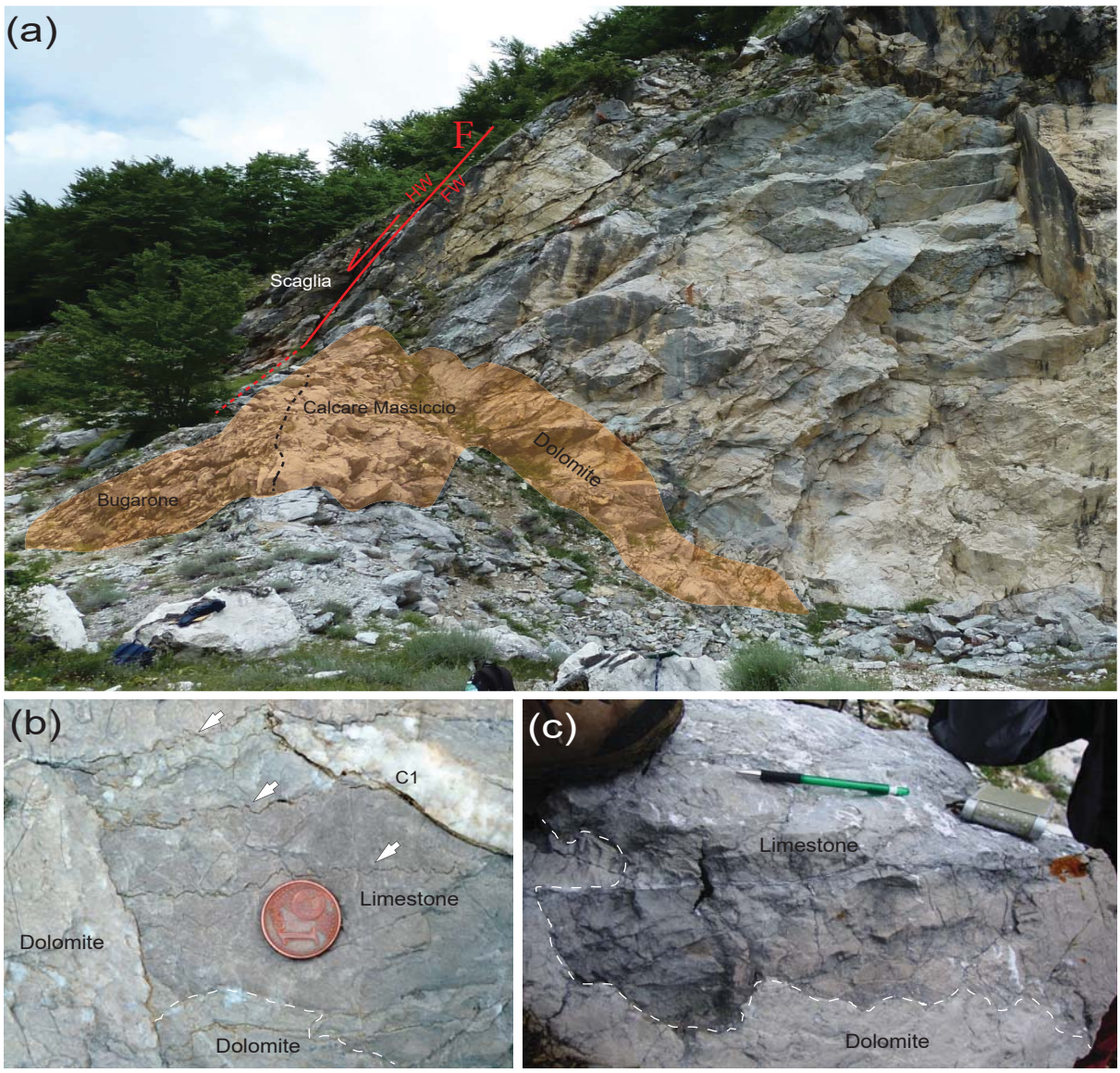
(a)
F
HW
FW
Scaglia
Calcare Massiccio
Dolomite
Bugarone
(b)
C1
Limestone
Dolomite
Dolomite
(c)
Limestone
Dolomite

Fig. 4

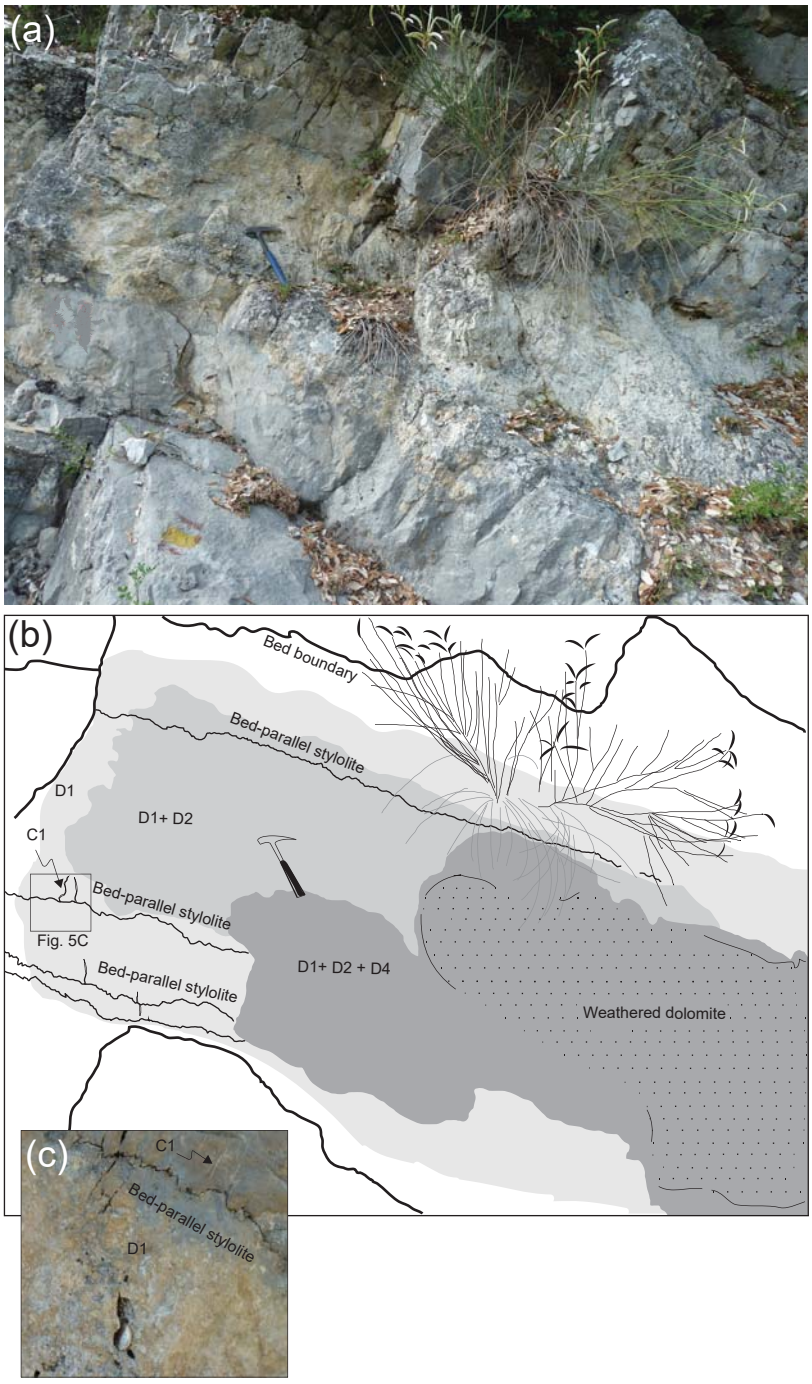
(a)
(b)
Bed boundary
Bed-parallel stylolite
D1
D1+ D2
C1
Bed-parallel stylolite
Fig. 5C
Bed-parallel stylolite
D1+ D2 + D4
Weathered dolomite
(c)
C1
Bed-parallel stylolite
D1

Fig. 5

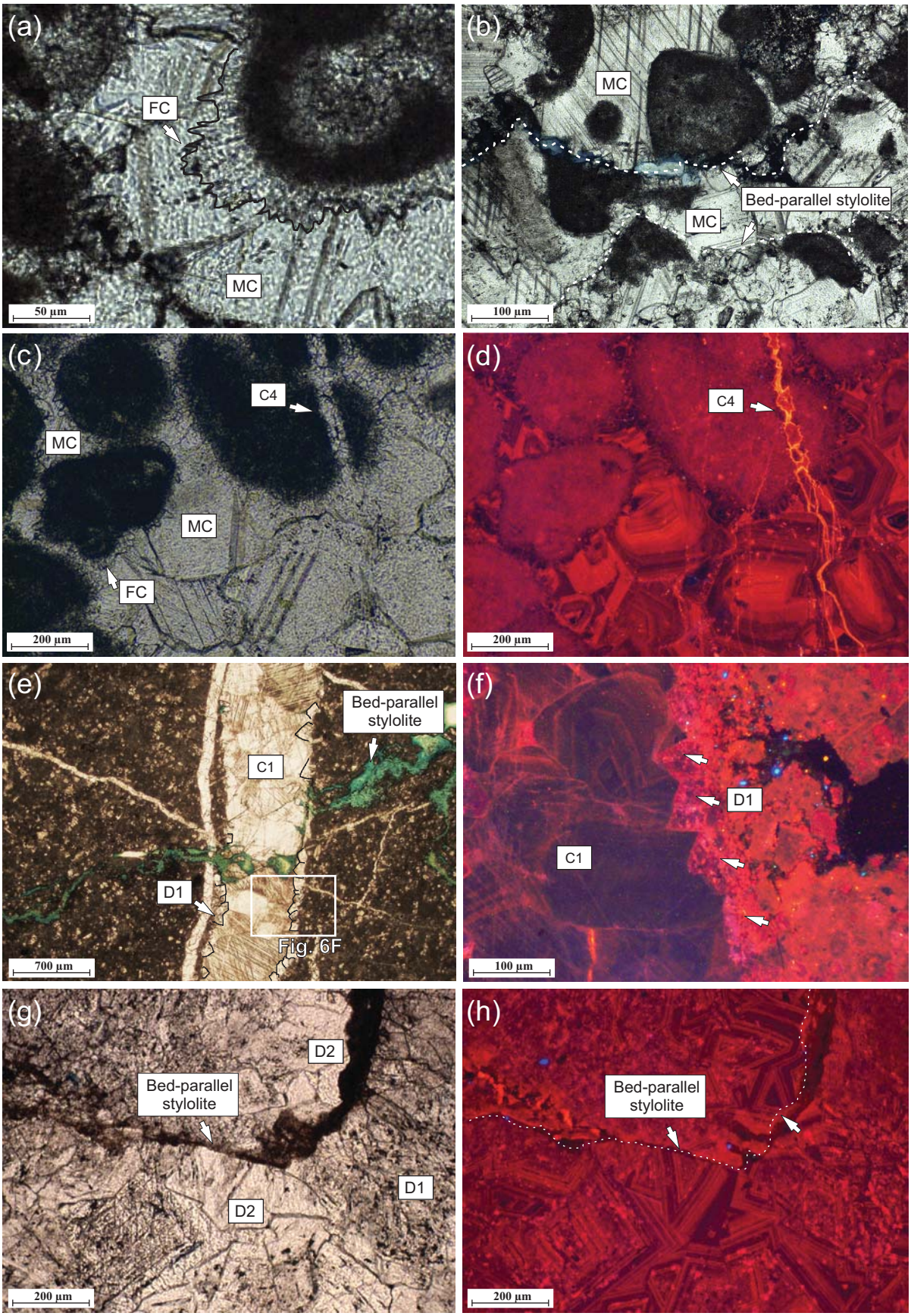
(a)
FC
MC
50 µm
(b)
MC
Bed-parallel stylolite
MC
100 µm
(c)
C4
MC
MC
FC
200 µm
(d)
C4
200 µm
(e)
Bed-parallel stylolite
C1
D1
Fig. 6F
700 µm
(f)
D1
C1
100 µm
(g)
D2
Bed-parallel stylolite
D1
D2
200 µm
(h)
Bed-parallel stylolite
200 µm

Fig. 6

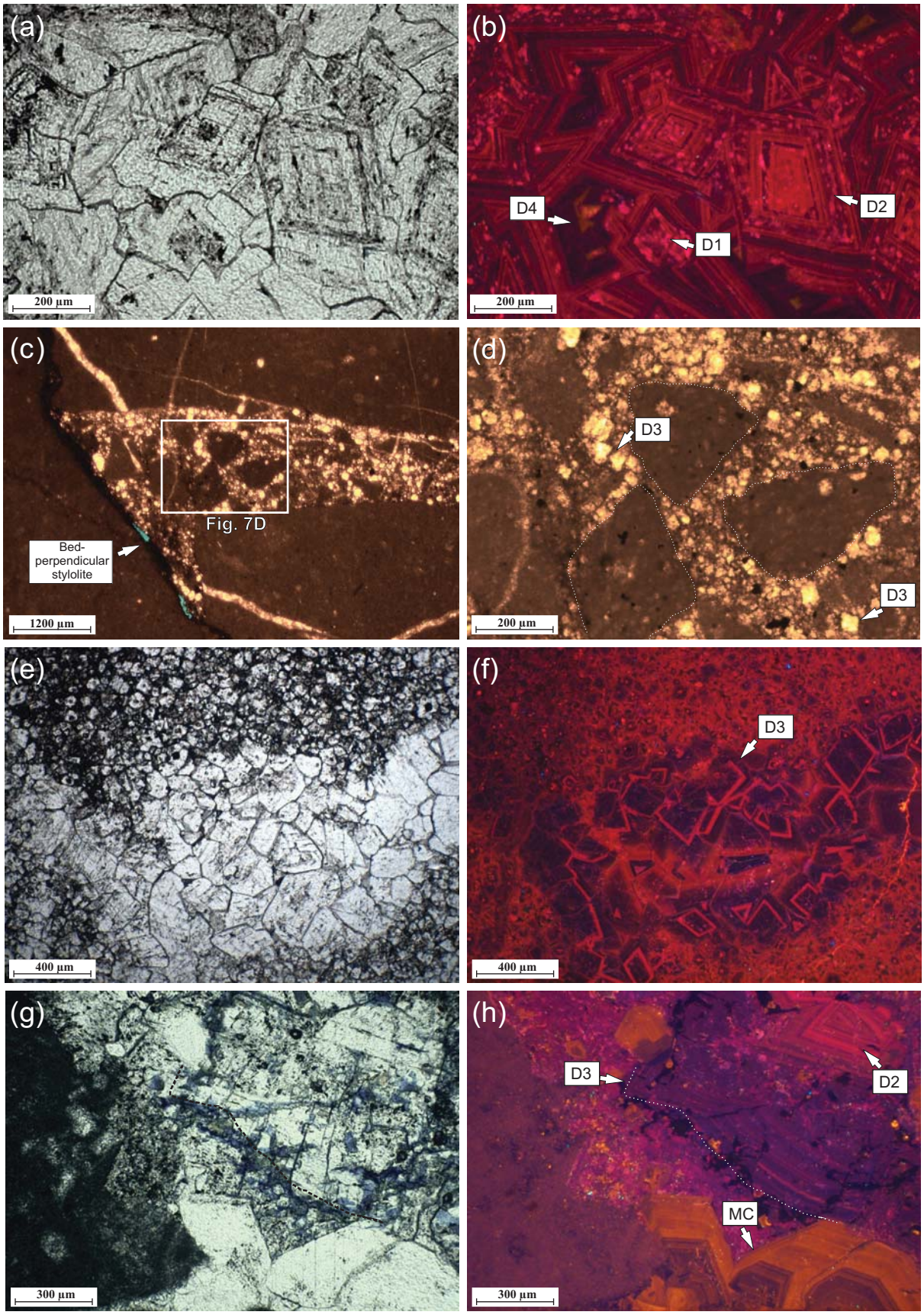
(a)
200 µm
(b)
D4
D2
D1
200 µm
(c)
Fig. 7D
Bed-perpendicular stylolite
1200 µm
(d)
D3
D3
200 µm
(e)
400 µm
(f)
D3
400 µm
(g)
300 µm
(h)
D3
D2
MC
300 µm

Fig. 7

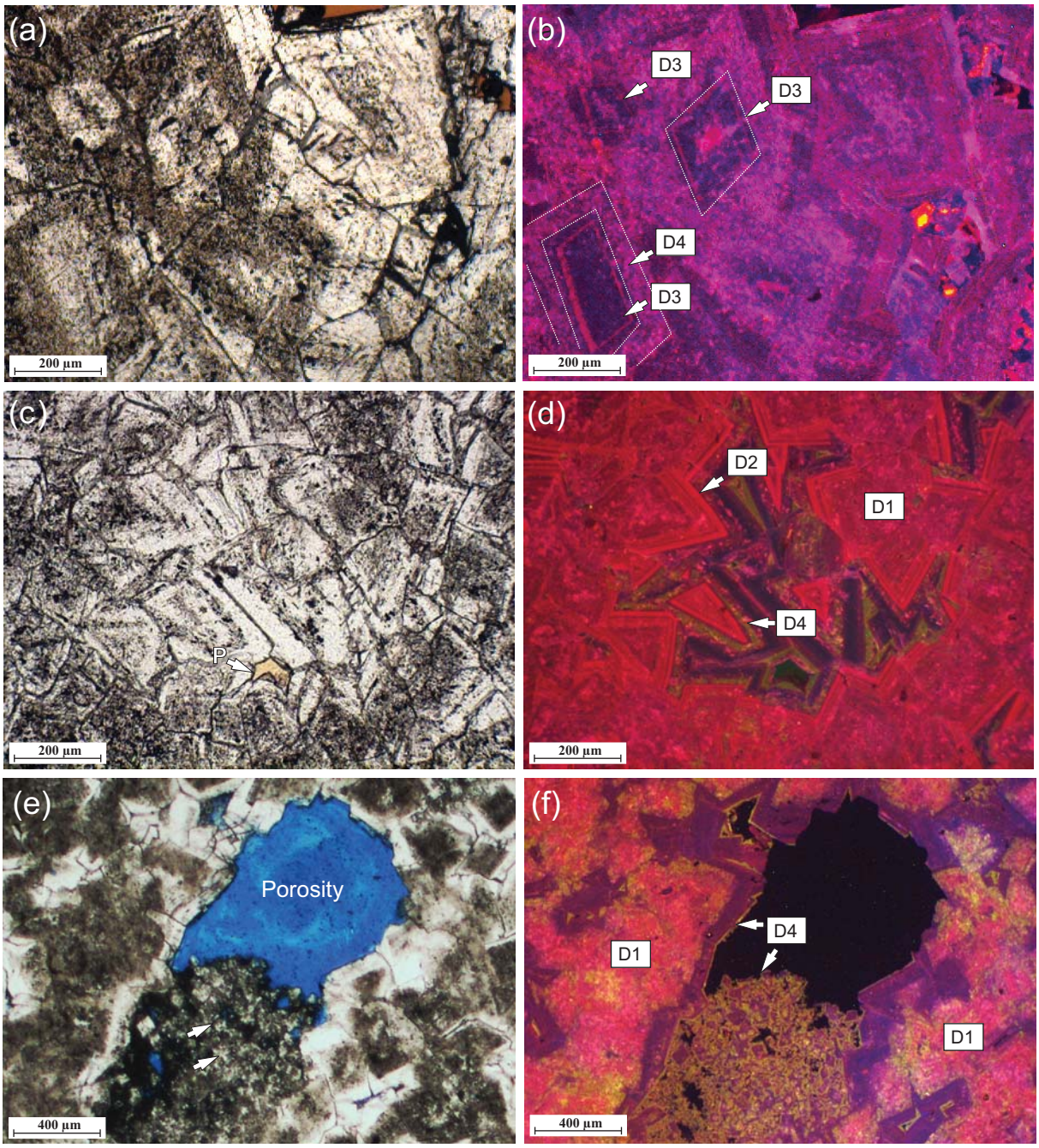
(a)
200 µm
(b)
D3
D3
D4
D3
200 µm
(c)
P
200 µm
(d)
D2
D1
D4
200 µm
(e)
Porosity
400 µm
(f)
D4
D1
D1
400 µm

Fig. 8

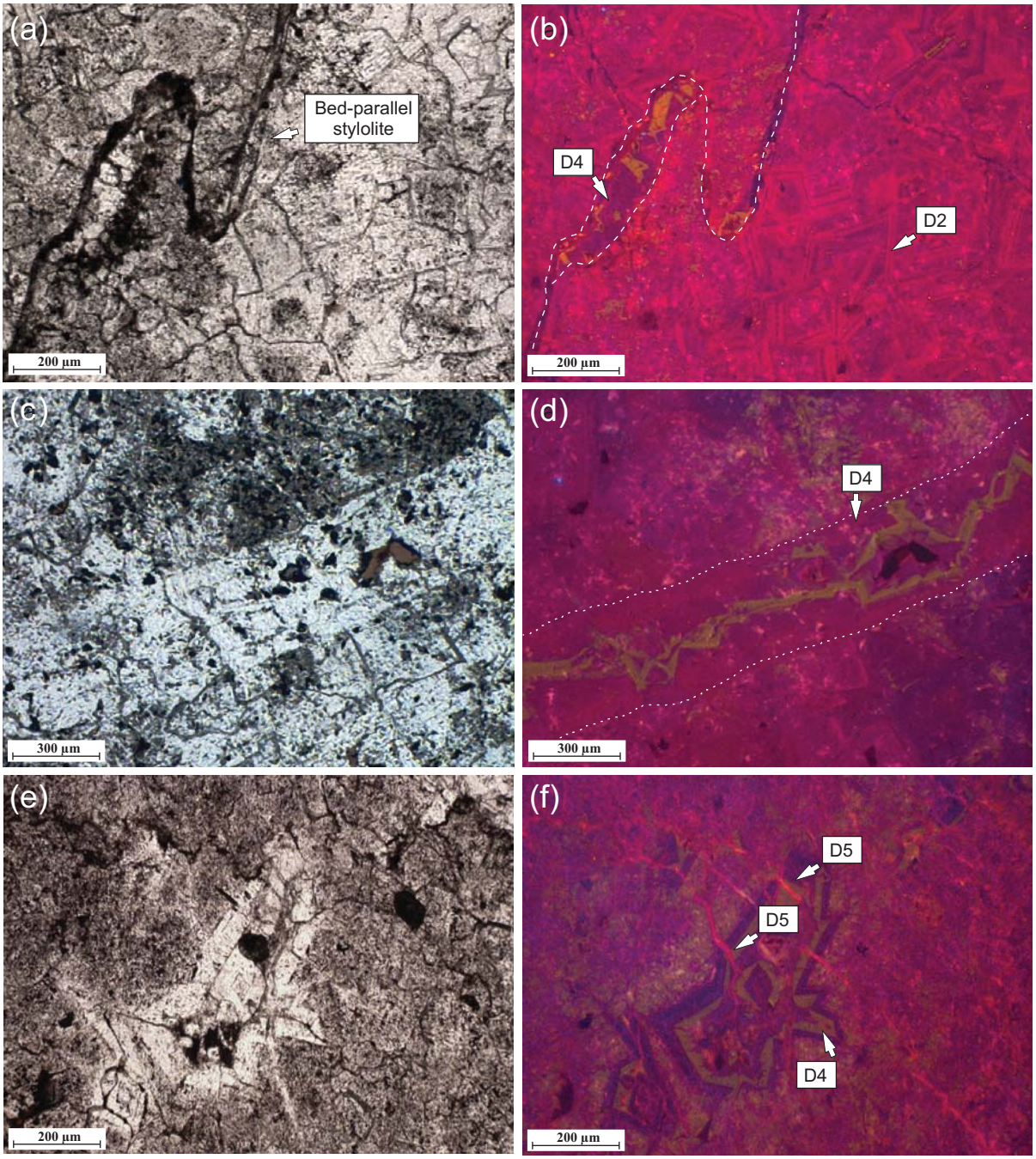
(a)
Bed-parallel stylolite
200 µm
(b)
D4
D2
200 µm
(c)
300 µm
(d)
D4
300 µm
(e)
200 µm
(f)
D5
D5
D4
200 µm

Fig. 9

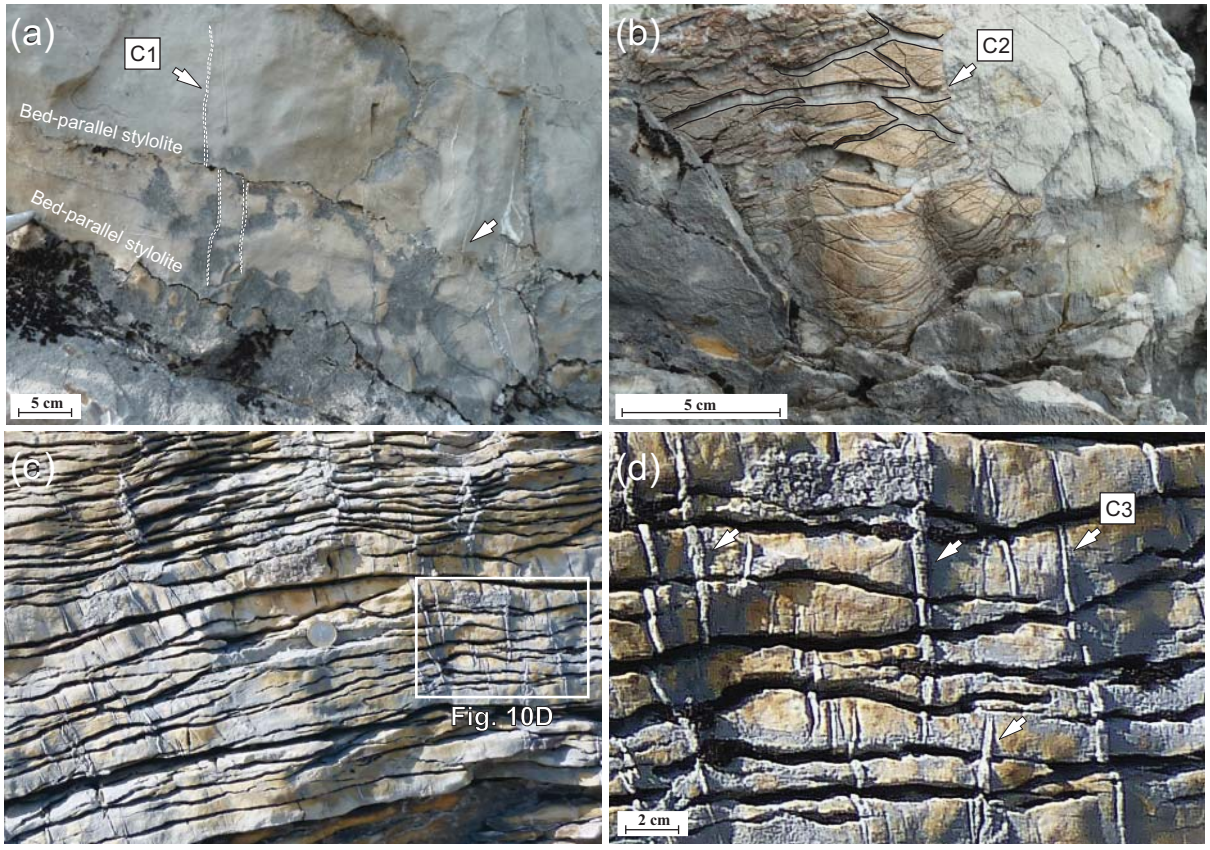
(a)
C1
Bed-parallel stylolite
Bed-parallel stylolite
5 cm
(b)
C2
5 cm
(c)
Fig. 10D
(d)
C3
2 cm

Fig. 10

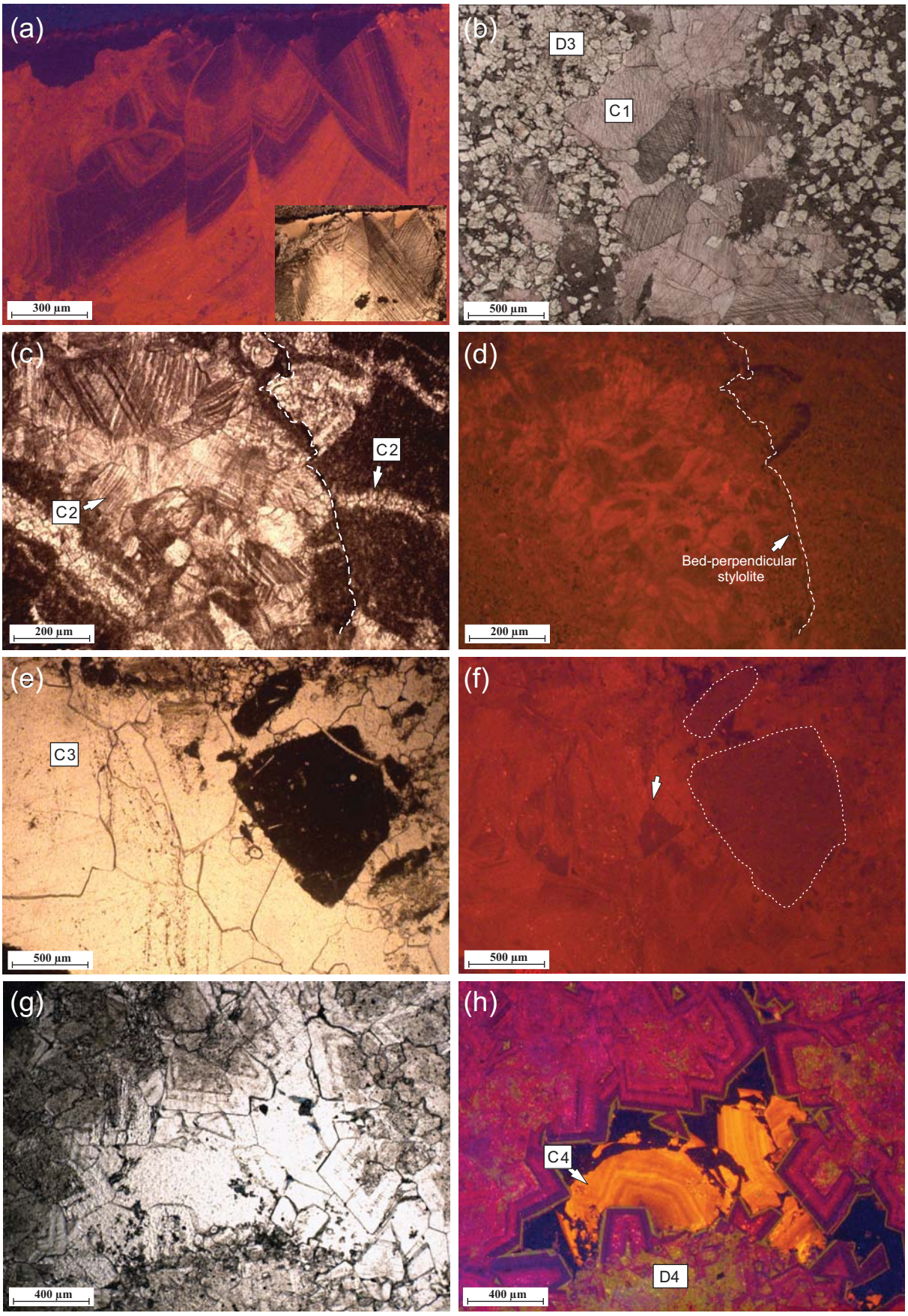
(a)
300 µm
(b)
D3
C1
500 µm
(c)
C2
C2
200 µm
(d)
Bed-perpendicular
stylolite
200 µm
(e)
C3
500 µm
(f)
500 µm
(g)
400 µm
(h)
C4
D4
400 µm

Fig. 11

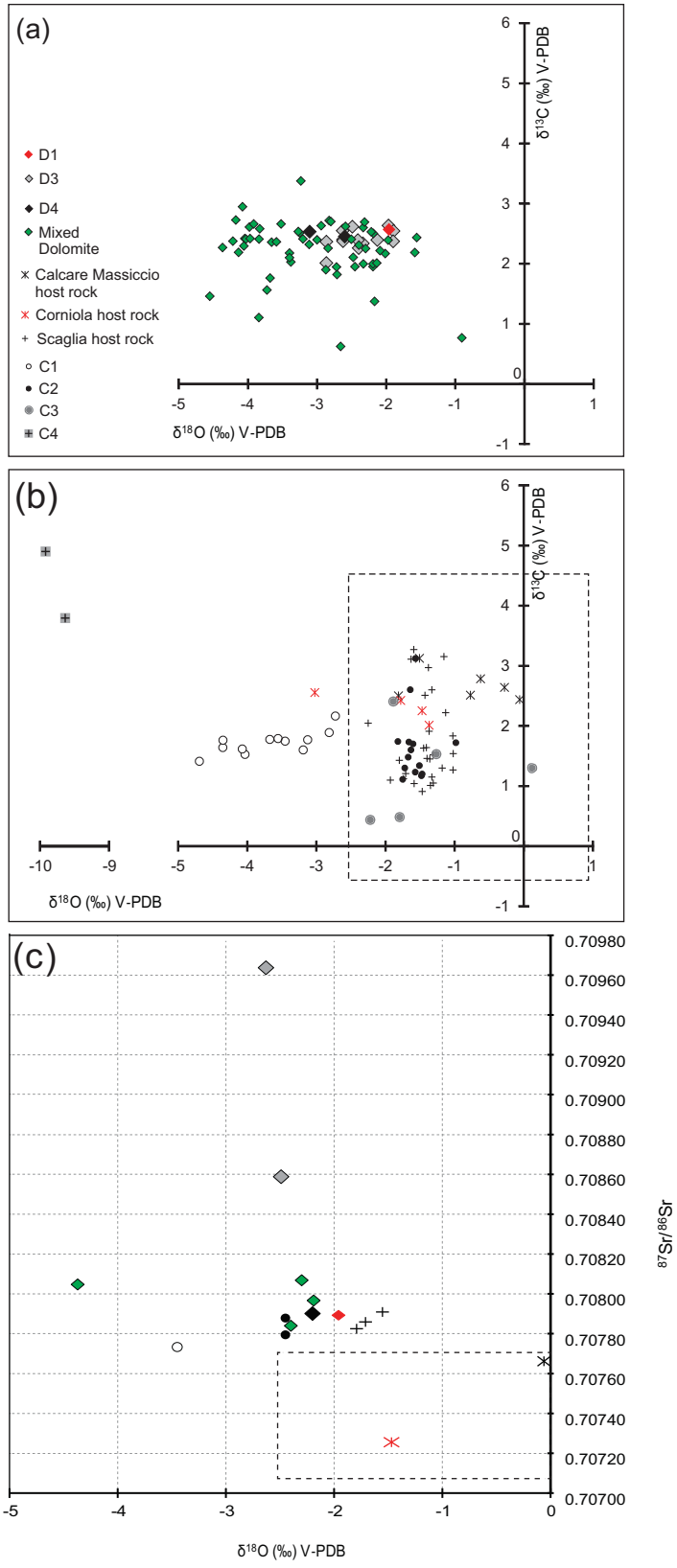
(a)
D1
D3
D4
Mixed Dolomite
Calcare Massiccio host rock
Corniola host rock
Scaglia host rock
C1
C2
C3
C4
δ13C (‰) V-PDB
δ18O (‰) V-PDB
(b)
δ13C (‰) V-PDB
δ18O (‰) V-PDB
(c)
87Sr/86Sr
δ18O (‰) V-PDB

Fig. 12

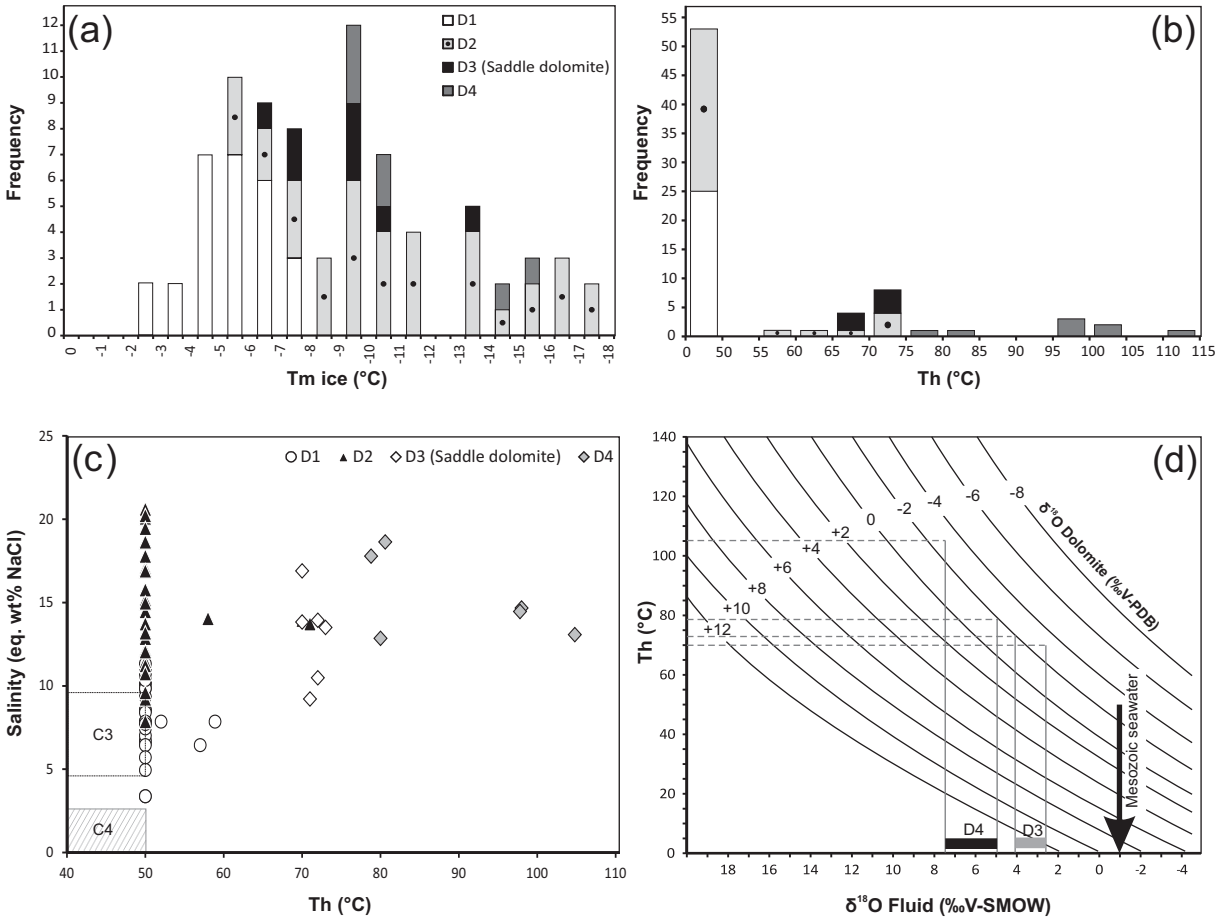
(a)
D1
D2
D3 (Saddle dolomite)
D4
Frequency
Tm ice (°C)
(b)
Frequency
Th (°C)
(c)
D1 D2 D3 (Saddle dolomite) D4
Salinity (eq. wt% NaCl)
C3
C4
Th (°C)
(d)
δ18O Dolomite (‰V-PDB)
Th (°C)
Mesozoic seawater
D4
D3
δ18O Fluid (‰V-SMOW)

Fig. 13

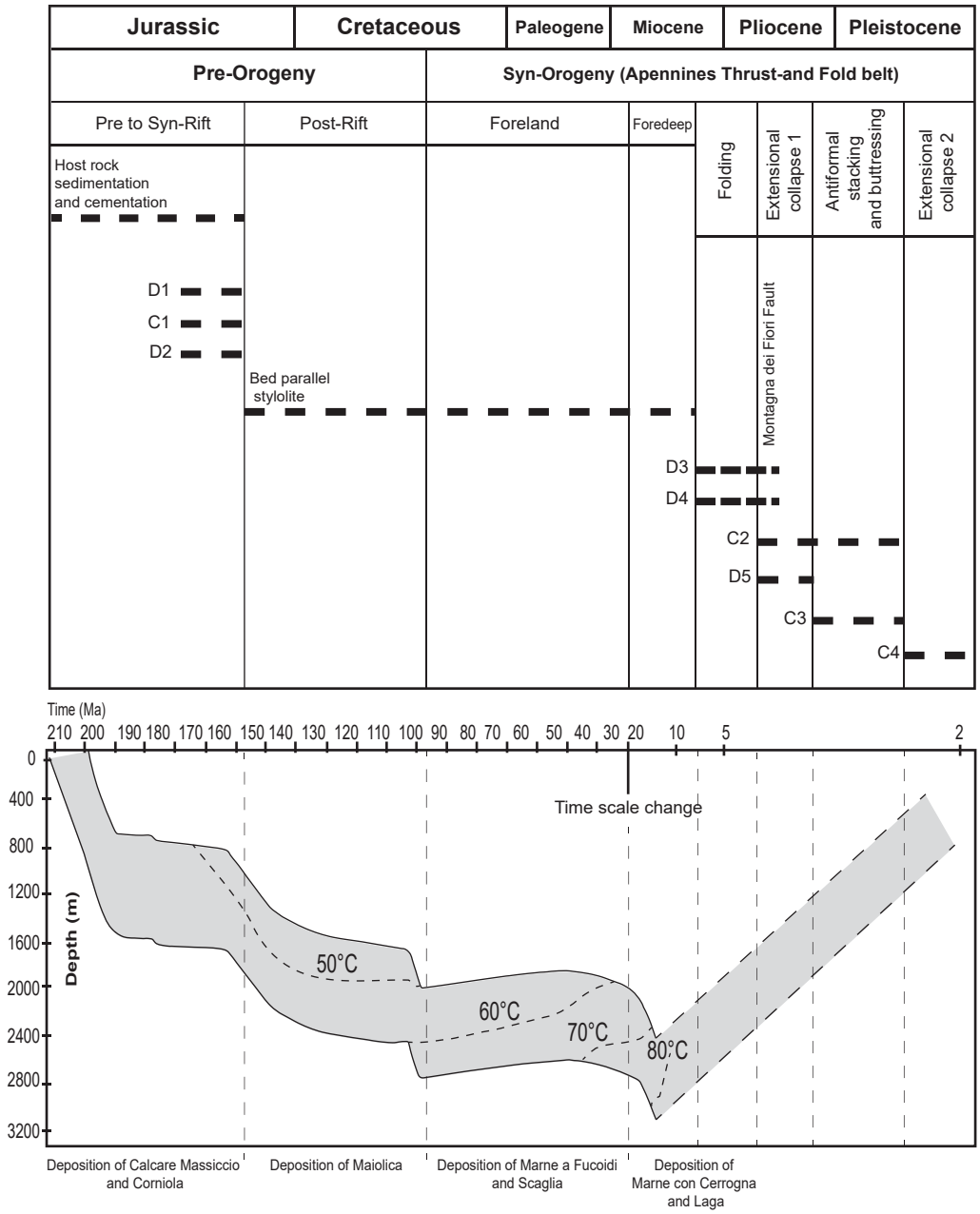
Jurassic
Cretaceous
Paleogene
Miocene
Pliocene
Pleistocene
Pre-Orogeny
Syn-Orogeny (Apennines Thrust-and Fold belt)
Pre to Syn-Rift
Post-Rift
Foreland
Foredeep
Folding
Extensional collapse 1
Antiformal stacking and buttressing
Extensional collapse 2
Host rock sedimentation and cementation
D1
C1
D2
Bed parallel stylolite
Montagna dei Fiori Fault
D3
D4
C2
D5
C3
C4
Time (Ma)
210 200 190 180 170 160 150 140 130 120 110 100 90 80 70 60 50 40 30 20 10 5 2
Time scale change
Depth (m)
0
400
800
1200
1600
2000
2400
2800
3200
50°C
60°C
70°C
80°C
Deposition of Calcare Massiccio and Corniola
Deposition of Maiolica
Deposition of Marne a Fucoidi and Scaglia
Deposition of Marne con Cerrogna and Laga

Fig. 14

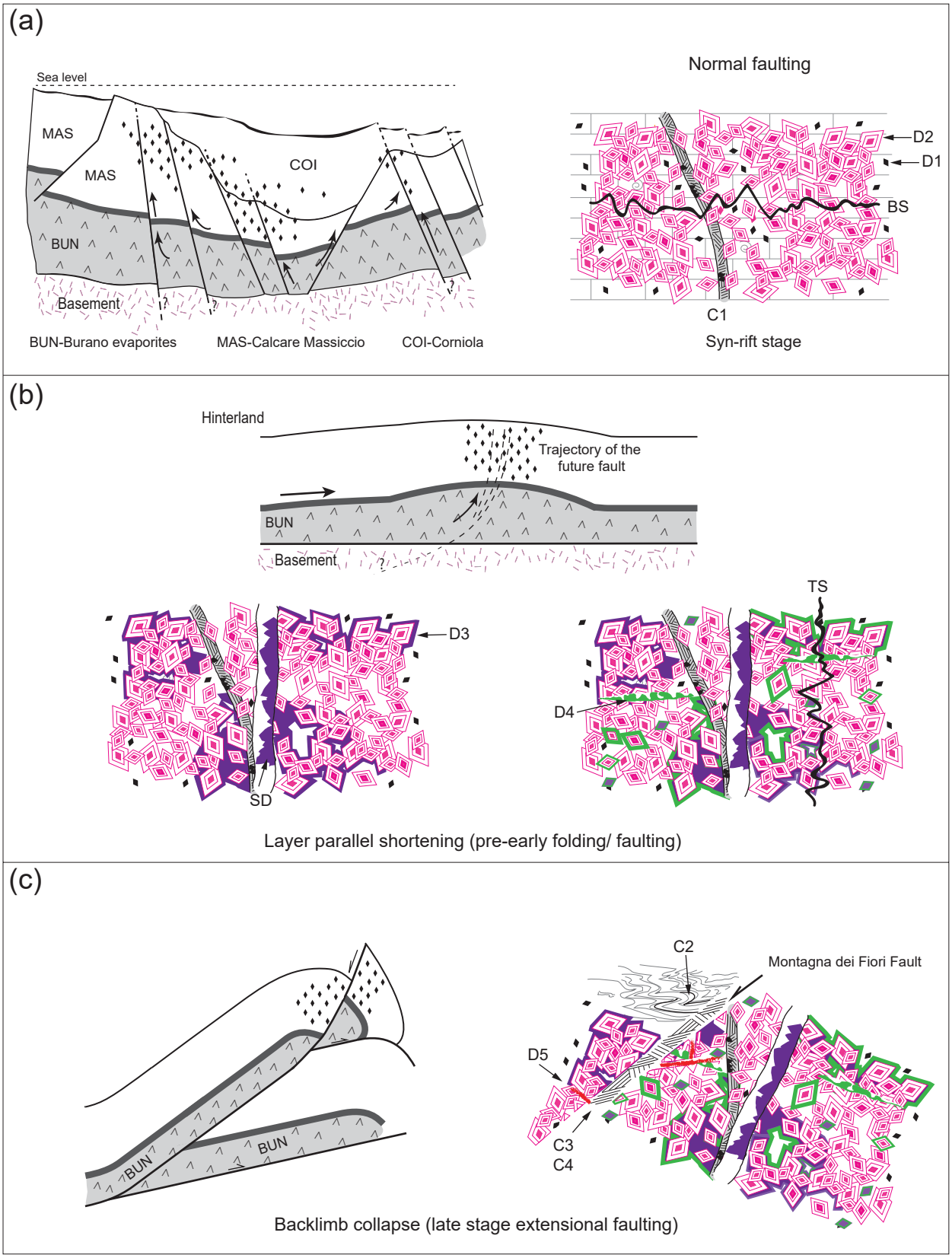
(a)
Sea level
MAS
MAS
COI
BUN
Basement
BUN-Burano evaporites
MAS-Calcare Massiccio
COI-Corniola
Normal faulting
D2
D1
BS
C1
Syn-rift stage
(b)
Hinterland
Trajectory of the future fault
BUN
Basement
D3
SD
TS
D4
Layer parallel shortening (pre-early folding/ faulting)
(c)
BUN
BUN
C2
Montagna dei Fiori Fault
D5
C3
C4
Backlimb collapse (late stage extensional faulting)

Fig. 15